AD NUMBER
AD039844
CLASSIFICATION CHANGES
TO: **unclassified**
FROM: **confidential**
LIMITATION CHANGES
TO: **Approved for public release; distribution is unlimited.**
FROM: **Distribution authorized to U.S. Gov't. agencies and their contractors; Administrative/Operational Use; 08 MAR 1954. Other requests shall be referred to Naval Ordnance Systems Command, Washington, DC.**
AUTHORITY
31 mar 1966, DoDD 5200.10; usnol ltr, 29 aug 1974

AD _____

NAVORD REPORT 3650

MEASUREMENTS OF BLOCKAGE AREA RATIO, PRESSURE DISTRIBUTION, AND BOUNDARY LAYER TRANSITION ON HOLLOW CYLINDERS

8 MARCH 1954

U. S. NAVAL ORDNANCE LABORATORY
WHITE OAK, MARYLAND

NAVORD Report 3650

Aeroballistic Research Report 226

MEASUREMENTS OF BLOCKAGE AREA RATIO, PRESSURE DISTRIBUTION, AND BOUNDARY LAYER TRANSITION ON HOLLOW CYLINDERS

Prepared by:

R. E. Lee

ABSTRACT: Wind tunnel tests were conducted to determine the feasibility of using hollow cylinder models for boundary layer measurements. The tests were conducted in the NOL 40 x 40 cm Aeroballistics Wind Tunnel No. 1 at Mach numbers from 2.2 to 5.0 on models that had either an inside or outside beveled leading edge. In these tests, inserts with smaller openings were placed inside the model to determine the blockage area permitted for the housing of a balance for measuring local skin friction. Both internal and external flows were surveyed by pitot and static pressure probes. Boundary layer transition locations on the inner and outer surfaces were measured with a surface probe. For the case of the outer surface, these data were compared with transition locations measured from schlieren photographs.

Blockage area ratios were investigated with the internal bevel model and were in close agreement with theory provided the displacement of the internal boundary layer was added to the obstruction. The particular shape of the obstruction appeared to have little effect on the shock-swallowing ability of the model. For the case of the external bevel model, pressure surveys indicated a slight adverse pressure gradient in the internal flow and also consecutive reflections of a weak disturbance originating at the leading edge. Measurements with the surface probe and on schlieren photographs showed a delay of boundary layer transition on the outer surface of the external bevel model.

The hollow cylinder is an ideal model for studying boundary layer characteristics. In attempting to obtain a surface with zero pressure gradient, the outer surface of an internal bevel model is superior if the wind tunnel flow is uniform. For poor wind tunnel flow, the best pressure distribution may be obtained on the inner surface of an external bevel model by proper location of the cylinder leading edge.

U. S. NAVAL ORDNANCE LABORATORY
WHITE OAK, MARYLAND

NAVORD Report 3650 8 March 1954

Presented in this report is the second phase of a series of feasibility studies on hollow cylinder models for direct local skin friction measurements. The experimental data were obtained during the calendar year of 1953 and early 1954 in the 40 x 40 cm Aeroballistics Wind Tunnel No. 1 at the U. S. Naval Ordnance Laboratory. The project was sponsored by the Naval Bureau of Ordnance under task number NOL-Re9a-108.

The author wishes to acknowledge the work of Mr. R. T. Schroth, who designed the models.

EDWARD L. WOODYARD
Captain, USN
Commander

H. H. KURZWEG, Chief
Aeroballistic Research Department
By direction

CONTENTS

	Page
Introduction	1
Equipment and Procedure	1
Discussion of Results	3
Conclusions	6
References	8

ILLUSTRATIONS

		Page
Figure 1.	Section Views of Hollow-Cylinder Models and Accessories	9
Figure 2.	Micrograph of Leading Edge Casting (1 scale division = .05 mm)	10
Figure 3.	Photograph of Dummy Balances and Expansion Section	11
Figure 4.	Cross-Sections of Dummy Balances	12
Figure 5.	Pressure Probes	13 & 14
Figure 6.	Schlieren Photograph of Flow on Model with Surface Probe at M = 3.25	15
Figure 7.	Photographs Showing Effect of Area Ratio on the "Swallowing" of the Bow Shock	16
Figure 8.	Schlieren Photograph of Internal Bevel Hollow Cylinder with Bow Shock not "Swallowed," M = 2.15	17
Figure 9.	Schlieren Photograph of Internal Bevel Hollow Cylinder with Bow Shock "Swallowed," M = 2.15	18
Figure 10.	Schlieren Photograph of External Bevel Hollow Cylinder with Bow Shock "Swallowed," M = 2.15	19
Figure 11.	Maximum Contraction Ratio to "Swallow" Bow Shock	20
Figure 12.	Pressure and Mach Number Distribution Along Centerline of Hollow Cylinder with 10° Internal Bevel and Bow Shock not "Swallowed," M = 2.15	21
Figure 13.	Pressure and Mach Number Distribution Along Centerline of Hollow Cylinder with 10° Internal Bevel and Bow Shock "Swallowed," M = 2.15	22
Figure 14.	Pressure and Mach Number Distribution Along Centerline of Hollow Cylinder with 10° External Bevel and Bow Shock "Swallowed," M = 2.15	23
Figure 15.	Pitot Pressures on Internal Bevel Hollow Cylinder at M = 2.15	24
Figure 16.	Pitot Pressures on External Bevel Hollow Cylinder at M = 2.15	25
Figure 17.	Pitot Pressures on Internal Bevel Hollow Cylinder at M = 3.25	26
Figure 18.	Pitot Pressures on External Bevel Hollow Cylinder at M = 3.25	27
Figure 19.	Shock Pattern Inside Hollow Cylinder Models at M = 2.15	28
Figure 20.	Shock Pattern Inside Hollow Cylinder Models at M = 3.25	29
Figure 21.	Static Pressure Distribution on Internal Surface of External Bevel Model	30
Figure 22.	Comparison of Static Pressure on Internal Surface of External Bevel Model with Static Pressure on External Surface of Internal Bevel Model in Terms of Pressure Ratio $\frac{p - \bar{p}}{p_o}$	31
Figure 23.	Comparison of Boundary-Layer Transition on the External Surface of Two Different Hollow Cylinder Models at Two Mach Numbers	32

SYMBOLS

A	Cross-section area of hollow cylinder based on outer diameter
A^*	Throat area of "dummy balance"
A^*/A	Blockage area ratio
A^{**}	A^* less boundary-layer displacement area
δ	Boundary-layer thickness
δ^*	Boundary-layer displacement thickness
M	Mach number
p	Static pressure
p_o	Supply pressure
p_o'	Pitot pressure
Re	Reynolds number based on distance from leading edge

MEASUREMENTS OF BLOCKAGE AREA RATIO, PRESSURE DISTRIBUTION AND BOUNDARY LAYER TRANSITION ON HOLLOW CYLINDERS

INTRODUCTION

1. The present investigation is the second of a series of tests of hollow cylinder models. The purpose as was stated in reference a is: "...feasibility studies aimed at the direct measurement of local laminar and turbulent skin-friction drag, boundary-layer profiles, recovery temperatures, and heat transfer characteristics on a model without pressure gradient." Skin-friction drag derived from temperature and pressure measurements at Mach number 3.05 on a similar hollow cylinder model is reported by Brinich and Diaconis, reference b. The cylinder data are consistent with flat plate theories of Wilson, reference c; Rubesin, Maydew and Varga, reference d. The advantages of hollow cylinder models over flat plate models for wind tunnel investigations were discussed in reference b and by the author in reference a.

2. One of the aims of this report was to determine the internal area permissible for the housing of a skin-friction balance inside the cylinder without choking the internal flow. This permissible blockage was determined by inserting restrictions of varying cross-sectional areas into the cylinder and checking optically with a schlieren system if the bow shock was "swallowed."

3. Due to mechanical difficulties in housing the above-mentioned balance inside the cylinder, the question arose whether it might be possible to house a balance outside the cylinder and measure the friction drag on the internal surface. To investigate this possibility, pressure surveys were made with pitot and static probes along the centerline of the cylinder and with a pitot probe along the internal and external surfaces at Mach numbers 2.15 and 3.25 on two hollow cylinders (the previously reported cylinder with an internal bevel and a new cylinder with an external bevel leading edge). In addition, static pressures on the inner surface of the external bevel model were measured at Mach numbers 2.15, 2.47, 2.86 and 3.25. Boundary-layer transitions detected on the outer surface with the surface probe were checked with transitions from schlieren photographs of the boundary layer.

EQUIPMENT AND PROCEDURE

4. All data were taken in the NOL Aeroballistics Wind Tunnel No. 1. This tunnel has a 40 x 40 cm test section and operates intermittently with a maximum duration of about one minute to each blow. Supply air is taken from the atmosphere, passed through dryers and the tunnel, and discharged into an evacuated sphere. A detailed description of the tunnel is found in reference e.

5. Figure 1 is a sectional view of the hollow-cylinder models used for this investigation. All three models are made of brass, having an outer diameter of 4 inches, an effective length (distance from leading edge of model to leading edge of support) of 19 inches, and a .062-inch wall thickness. Model (a) has a 10° internal bevel at the leading edge and models (b) and (c) have 10° external bevel leading edges. Model (a) was used for the shock "swallowing" investigation, models (a) and (b) were used for pitot pressure and static pressure measurements (along centerline) and boundary-layer transition investigations while model (c) was used solely for measuring the static pressure distribution on the inside surface. Model (c) has ten .080" inner diameter static pressure taps located on the internal surface at 1, 3, 5, 7, 9, 11, 13, 15, 17 and 18.5 inches from the leading edge. Each tap is offset circumferentially 20° from the preceding tap as shown in Figure 1.

6. Surface roughness of the models was measured in microinches, r.m.s., with a profilometer made by the Physicists Research Company. Model (a) averaged about 20 microinches on the outer surface and 18 microinches on the inner surface. Model (b) averaged about 15 microinches on the outer surface and 17 microinches on the inner surface. Model (c) averaged roughly 26 microinches on the inner surface. The roughness measurements on the inner surface were fairly uniform over the whole length of the model with the maximum roughness less than 32 microinches. The roughness on the outer surface of models (a) and (b) was greater at both ends with the maximum less than 60 microinches.

7. The radius of curvature of the sharp leading edges of the three models was determined from bakelite castings made of the annular leading edges. Each casting was cut on a milling machine so that two of its sides were perpendicular to the impression of the leading edge. The measurements of the impression of the leading edge on the polished surface were then made with a calibrated microscope. Figure 2 is a microphotograph of a typical casting of the model leading edge. The leading edge radius of model (a) is .00062" ± .00022"; of model (b), .00077" ± .00044"; and of model (c), .00122" ± .00038".

8. The models were mounted in the tunnel such that the axis of the hollow cylinder coincided with the centerline of the tunnel within a tolerance of three minutes. Two types of mount were used to support the models. Originally a center support mount was used, Figure 1-a. This mount has four side openings permitting a total exit area of approximately three times the cross-sectional intake area at the leading edge. The sting is directly on the axis of the cylinder. Due to the belief that the aft portion of this mount added to the choking of the internal flow, a second mount was made with a straight open channel and an off-axis sting bent at an angle of 17° to the axis on the vertical plane, also shown in Figure 1-b.

9. The flow into the hollow cylinder was restricted by three "dummy balances," A, B and C, Figures 3 and 4. The dummy balances (representing the shell for housing a skin-friction balance) are made of aluminum, 6

inches in length with a 15° internal bevel at the leading edge and a 7° aft taper (see Figure 1-b). The restricting area is determined by the wall thickness of the dummy balance. Figure 4 is a cross-sectional drawing of each type together with its effective area. Type A is completely cylindrical, type B consists of three internal ribs spaced 120° apart with connecting members between the ribs, and type C consists of only the three ribs. Types A and B are made to slide into the hollow cylinder on two "O" rings and fixed to the cylinder by set screws. Type C is mounted by attaching each rib directly to the inner wall of the cylinder.

10. Three methods were tried to induce the swallowing of the bow shock in cases where the shock was not swallowed but very close to being swallowed. First a subsonic diffuser was used at the rear of the cylinder in an attempt to expand the internal flow. Second, a stream of compressed air was ejected near the inner surface and close to the trailing edge, having a setup similar to that used in an induction wind tunnel. Third, a diaphragm was placed across the front opening of the cylinder and broken immediately after external flow had been established, hoping that the sudden change in pressure would force the shock through the model.

11. Figure 5-a is a drawing of the pitot probe and static probe attachment used for measuring the pressure distribution along the centerline of the models. The static probe attachment slid directly over the tip of the pitot probe. Pressures were measured with a mercury manometer.

12. Pitot pressure distributions one inch from the centerline and on the inside and outside surfaces were measured with the three-fingered probe shown in Figure 5-b. Figure 6 is a schlieren photograph of the surface probe with the orifice well within the laminar boundary layer. Due to the longer response time caused by the small orifice of the surface probe (see dimensions in Figure 5-c) the Statham gauge together with a servo-system indicator (designed by J. M. Kendall of NOL) replaced the mercury manometer. This second method decreased the volume of air in the system and in turn reduced the response time.

13. Static pressure distributions on the inner surface of the external bevel model were measured with a bank of mercury manometers designed by J. M. Kendall for the intermittent tunnels. A detailed description of this apparatus together with the single column manometer is contained in reference f.

14. Spark schlieren photographs of approximately one microsecond exposure time were taken of the models in the tunnel. A swallowed bow shock was indicated by the absence of the shock wave in front of the model as shown on photographs of Figure 7. The beginning of boundary-layer transition was determined on the photographs as the point where the smooth laminar portion breaks up into a turbulent structure (indicated by arrows in Figures 8, 9 and 10).

DISCUSSION OF RESULTS

15. Figure 11 is a comparison between the minimum area ratio inside the hollow cylinder producing a swallowed front shock and the starting area

ratio of a diffuser determined from the one-dimensional non-viscous energy relation, references g and h. The experimental data represent the minimum throat area ratios with the dummy balances located in the most downstream position inside the cylinder (the front shoulder of the dummy balance 20 inches downstream from the leading edge of the cylinder). These area ratios are approximately 7 percent higher than the theoretical values. A better agreement between the two is obtained by subtracting the displacement area of the turbulent boundary layer from the throat area of the dummy balance at the flow conditions just before the shock is swallowed, i.e., the Mach number is assumed to be one. The theoretical displacement thickness from reference i is:

$$\delta^* = \frac{.046\ x}{\sqrt[5]{Re_x}}$$

where $x = 20$ inches

The resulting area is $A^{**} = \pi(r^* - \delta^*)^2$

where $r^* = \sqrt{\frac{A^*}{\pi}}$

The data corrected for boundary layer are plotted as the dark points in Figure 11 and are in close agreement with the theoretical curve. It seems that the cross-sectional area of an obstruction is of prime importance and that its particular shape has little effect.

16. At Mach number 4.28 it was found that the bow shock was swallowed with a dummy balance in the upstream position (front shoulder 2 1/2 inches downstream from the leading edge of the cylinder) but was not swallowed with the same dummy balance placed at the downstream position inside the cylinder. The choking at the latter position was caused by the increase in boundary layer thickness on the inside surface. The expansion section, the air ejector and the diaphragm were applied with the dummy balance located in this latter position but none of the three methods affected the swallowing of the shock.

17. Static and pitot pressure distributions along the centerline of the model are shown in Figures 12, 13 and 14. The data were converted to Mach number by the Rayleigh pitot-tube relation. Figure 12 shows that when the bow shock was not swallowed inside the internal bevel model, the internal flow was subsonic. Figure 13 shows strong reflected disturbances inside the internal bevel model when the shock was swallowed. Figure 14 shows weak reflected disturbances inside the external bevel model. The Mach number variation after the initial shock (4 inches from the leading edge) was approximately 4 percent.

18. Longitudinal pressure surveys with a pitot probe one inch from the centerline and with a surface probe directly in contact with the inner and outer surfaces of both internal and external bevel models at M = 2.15

and M = 3.25 are plotted in Figures 15, 16, 17 and 18. For comparison, the pitot pressure distribution on the centerline is repeated in the figures.

19. Boundary-layer transition locations detected with the surface probe on outer surfaces agreed fairly well with transition location measured on schlieren photographs as shown in Figures 15 through 18. The pressure, detected by the surface probe, in the transition region was fluctuating; while in the laminar and turbulent regions, the pressure was steady.

20. Pressure measured with a surface probe in direct contact with the surface is somewhat higher in the laminar section of the boundary layer on the inner surface than in the laminar section of the outer surface as seen in Figure 16. This is contrary to the boundary layer theory that the layer is thicker on the inner surface. This disagreement arises from the geometry of the surface probe in respect to the curvature of the cylinder. Taking an hypothetical condition where the outer annular edge of the boundary layer strikes the rectangular orifice of the probe at points A, B and C as drawn in Figure 5-c, the portion of the layer scooped by the probe is enclosed by the arc ABC and the edge of the probe in contact with the model (shaded areas). By drawing chords AB and BC, dividing the rectangle into triangles, it can be seen that the probe scoops more of the free-stream flow on the inner surface than on the outer surface, the difference being twice the flow enclosed by the arc ABC and the chords AB and BC. The difference in pressure on the two surfaces is not as large at Mach number 3.25 due to a thicker boundary layer.

21. Regions of boundary layer transition on the outer surface of the models were located at approximately the same distance from the leading edge as the distance where the leading edge shock would strike the inner surface. Whether the shock on the inside surface had any influence on transition on the outside surface (heat conduction through the wall of the cylinder) will be investigated in the near future on insulated hollow cylinder models.

22. The location of the shock waves inside the cylinders have been estimated from the pitot pressure data inside the cylinders. These shock patterns are drawn in Figures 19 and 20. The estimates were based on the following three assumptions:

a. The shock is indicated by a sharp rise in the pressure. The assumed boundary of the shock is determined from pressure measurements at three consecutive stations where the shock is detected at the second station. This limit is represented by the horizontal bar in Figures 15 through 20.

b. The leading edge shock wave is conical.

c. The angle of incidence of the shock wave on the inner surface is equal to its reflected angle.

23. Figure 21 is a graph of the static pressure distribution on the inner surface of an external bevel hollow cylinder model at Mach numbers 2.15, 2.47, 2.86 and 3.25. A slight adverse pressure gradient along the inner surface was noted at all four Mach numbers. These data are compared, in Figure 22, to the static pressure distribution on the outer surface of the internal bevel model. The pressure distributions on the outer surface of the internal bevel model were found to be in good agreement with distributions measured in the clear tunnel (reference a).

24. Transition from laminar to turbulent boundary layer on the external surface is represented graphically in Figure 23. Transition as it is seen in schlieren photographs is the point where the smooth laminar layer suddenly disperses into a diffused thicker layer (see Figures 8, 9 and 10). The travel of this point is represented by the partially shaded areas of the graphs. Each transition region represents results from at least twelve transition observations. It should be noted that there is a pronounced delay in transition on the external bevel model. Transition Reynolds number increases from 1.2×10^6 to 1.8×10^6 at Mach number 2.15 and from 1.4×10^6 to 2.2×10^6 at Mach number 3.25. This more stable boundary layer may be due to the favorable pressure gradient over the shoulder of the model. Also the apparent location of the leading edge shock on the internal surface should not be overlooked since, as pointed out in paragraph 21, the initial shock of the internal bevel model may trip the outer boundary layer and causes early transition on the outside surface.

25. The increase in boundary layer stability caused by the shoulder of a cone-cylinder was noted previously in comparing transition Reynolds number of cone and cone-cylinder models tested at NOL. The shoulder effect may therefore be the principal cause of transition delay on the cylinder. In the graph of transition Reynolds number vs Mach number in Figure 8 of reference a, transition Reynolds number of the cone-cylinder is somewhat higher than that of the cone. Transition on the cone-cylinder model was located on the cylindrical portion behind the shoulder. A report of this phenomenon was made in the IAS Journal, reference k. A related effect was presented at the Twenty-second Annual Meeting of the IAS titled: "The Transition from a Turbulent to Laminar Boundary Layer" by J. Sternberg, Ballistic Research Laboratory, Aberdeen Proving Ground, Maryland.

CONCLUSIONS

26. The hollow cylinder is an ideal model for studying boundary layer characteristics. In attempting to obtain a surface with zero pressure gradient, the outer surface of an internal bevel model is superior if the wind tunnel flow is uniform. For poor wind tunnel flow, the best pressure distribution may be obtained on the inner surface of an external bevel model by proper location of the cylinder leading edge. Pressure surveys inside an external bevel model show an adverse pressure gradient along the inner surface and also disturbances from the leading edge. Regions free of these disturbances can be located inside the cylinder.

27. The maximum blockage area ratio permissible for a "swallowed" bow shock wave and available for the housing of a skin friction balance in a hollow cylinder is approximately 15 percent of the cross-sectional area at Mach number 2.2 and increases to about 30 percent at Mach number 5.0. These figures agree very well with the theoretical values for the starting area of a supersonic diffuser provided a correction for the displacement of the boundary layer is added to the blockage area.

28. A downstream shift of the boundary layer transition location on the model is produced by a discontinuity of the model contour. Observations of schlieren photographs showed that with a 10° shoulder shortly downstream of the leading edge, the shift corresponds to an increase of transition Reynolds number from 1.2×10^6 to 1.8×10^6 at Mach 2.2 and from 1.4×10^6 to 2.2×10^6 at Mach 3.3. Transition location determined from a surface probe in direct contact with the external surface agreed with transition location measured on schlieren photographs.

REFERENCES

a. Lee, R. E., "Measurements of Pressure Distribution and Boundary-Layer Transition on a Hollow-Cylinder Model", NAVORD Report 2823, 28 April 1953

b. Brinich, P. F., and Diaconis, N. S., "Boundary Layer Development and Skin Friction at Mach Number 3.05", NACA TN 2742, July 1952

c. Wilson, R. E., "Turbulent Boundary Layer Characteristics at Supersonic Speeds - Theory and Experiment", CM-569, DRL-221, Defense Research Laboratory, University of Texas, November 21, 1949

d. Rubesin, M. W., Maydew, R. C., and Varga, S. A., "An Analytical and Experimental Investigation of the Skin Friction of the Turbulent Boundary Layer on a Flat Plate at Supersonic Speeds", NACA TN 2305, 1951

e. Lightfoot, J. R., "The Naval Ordnance Laboratory Aeroballistic Research Facility," NOLR Report 1079, 15 August 1950

f. Kendall, J. M., "Equipment and Techniques for Making Pressure Measurements in Supersonic Wind Tunnels in Mach Numbers Up to 5", NAVORD Report 2580, 11 August 1952.

g. Eggink, G., "Deutsche Luftfahrtforschung," Forschungsbericht No. 1756 (1943)

h. Kantrowitz, A. and Donaldson, C. Du P., NACA Wartime Report No. L-713 (1945)

i. Schlichting, H., "Lecture Series on Boundary-Layer Theory, Part II," NACA TN No. 1218, April 1949

j. Lange, A. H. and Gieseler, L. P., "Measurement of Boundary-Layer Transition on a Standard Model to Determine the Relative Disturbance Level in Two Supersonic Wind Tunnels," NAVORD Report 2753, Naval Ordnance Laboratory, White Oak, Maryland, February 1953 (see Figure 9)

k. Lange, A. H. and Lee, R. E., "Note on Boundary-Layer Transition in Supersonic Flow," Journal of the Aeronautical Sciences, Volume 21, No. 1, January 1954

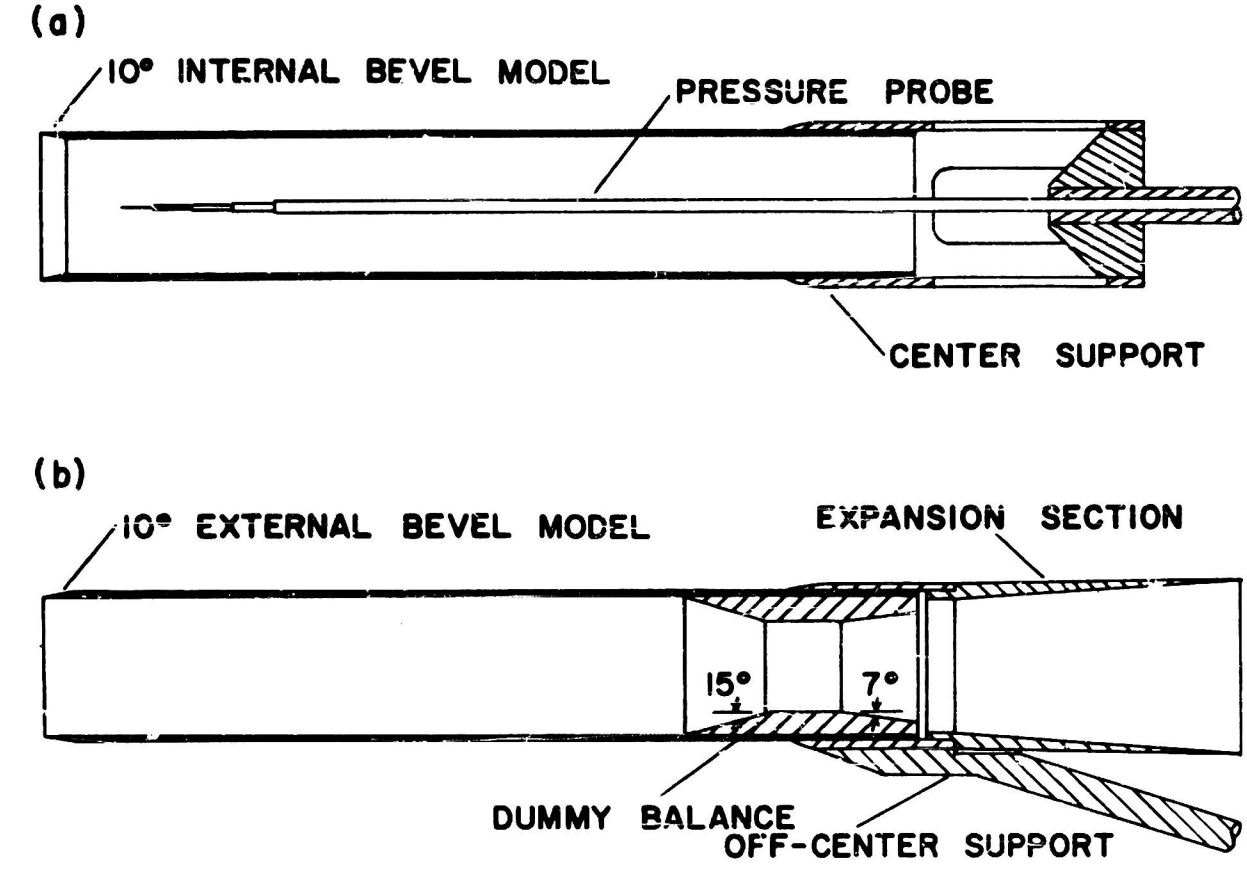

FIG. 1 SECTION VIEWS OF HOLLOW CYLINDER MODELS AND ACCESSORIES

FIG. 2 MICROGRAPH OF LEADING EDGE CASTING - 1 SCALE DIVISION = .05 mm.

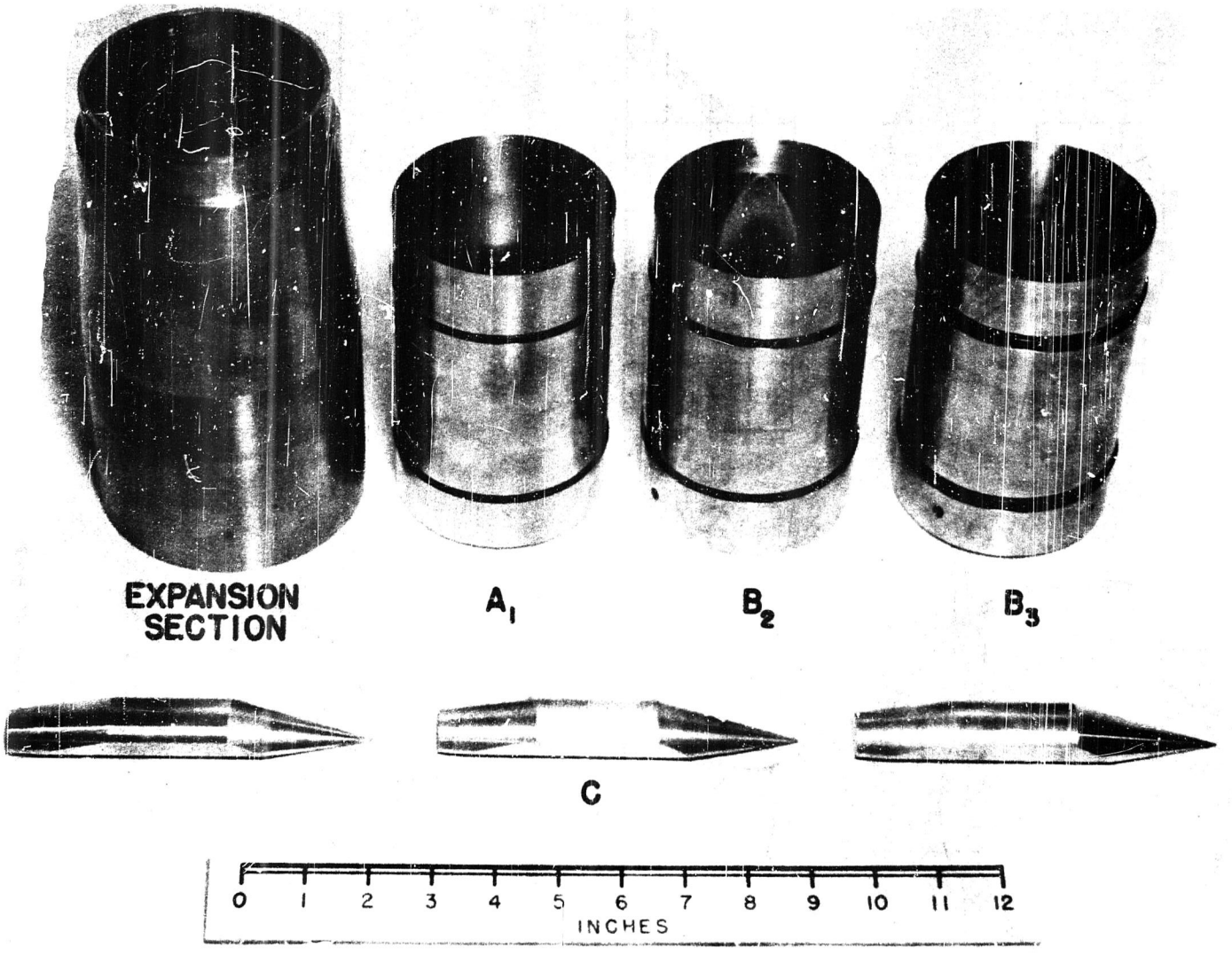

FIG. 3 PHOTOGRAPH OF DUMMY BALANCES & EXPANSION SECTION

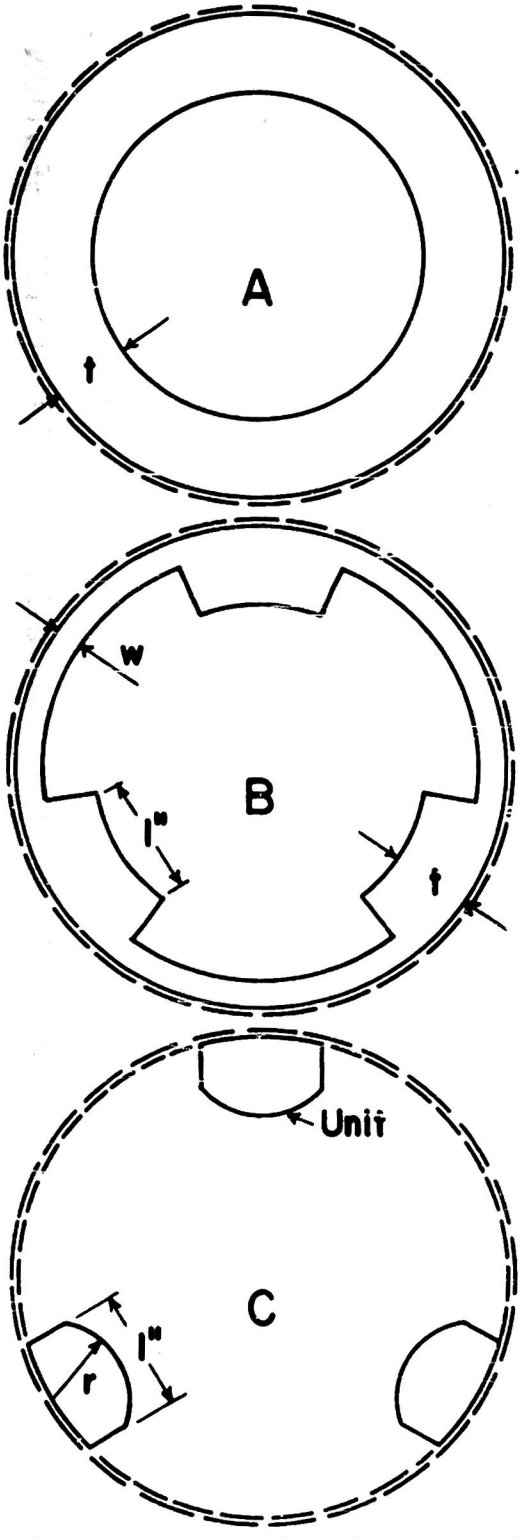

A	t	A*/A
1	.625	.431
2	.500	.517
3	.438	.562
4	.375	.611

B	t	w	A*/A
1	.625	.156	.666
2	.500	.156	.696
3	.375	.188	.707

C	r	Units	A*/A
1	.600	3	.797
2	.600	2	.845
3	.600	1	.893

t, w & r in inches

FIG. 4 CROSS-SECTIONS OF DUMMY BALANCES

(a) Centerline Probes

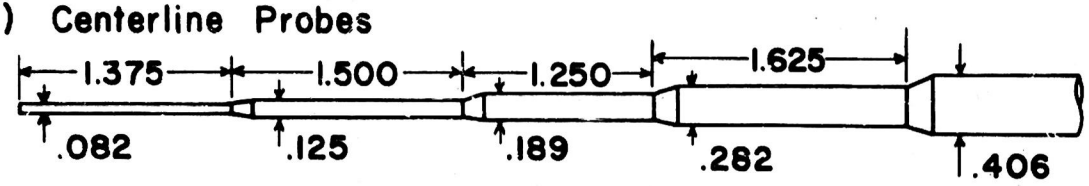

PITOT PROBE

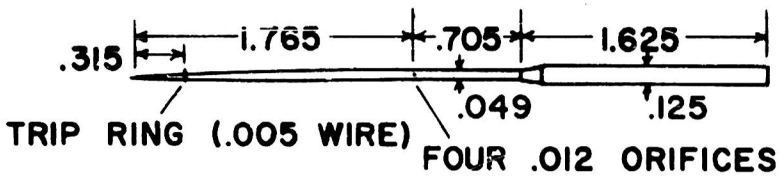

STATIC PROBE
(ATTACHED TO FRONT OF PITOT PROBE)

(b) Three Finger Probe

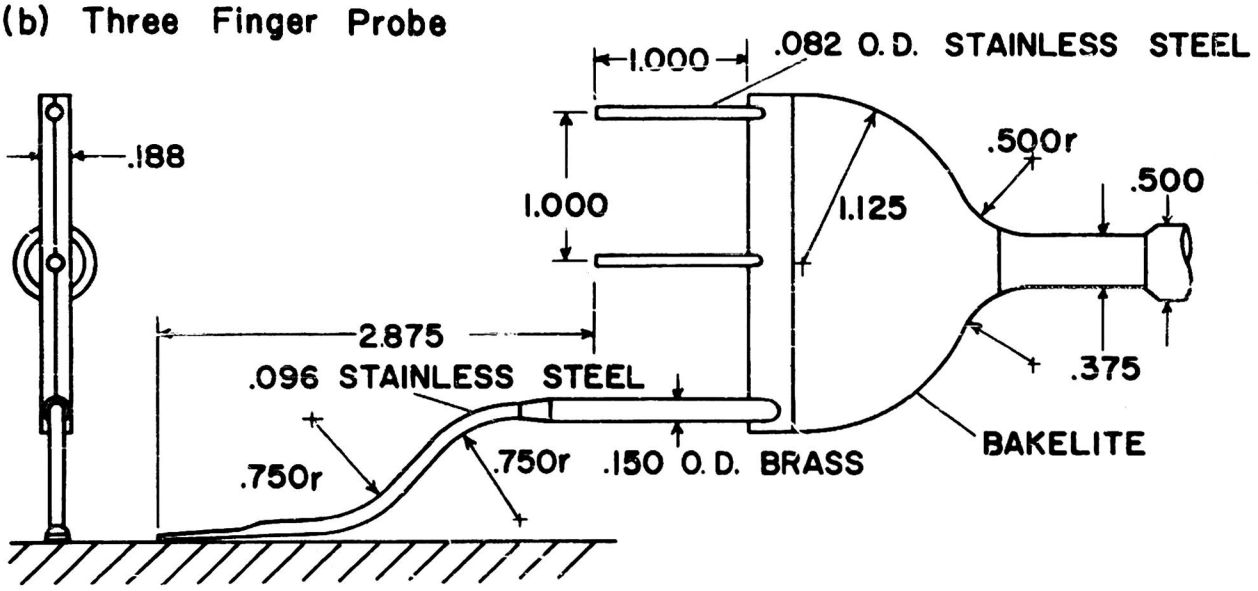

FIG. 5 PRESSURE PROBES ALL DIMENSIONS IN INCHES

(c) Surface Probe

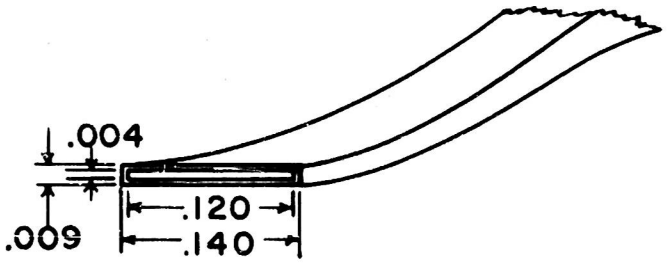

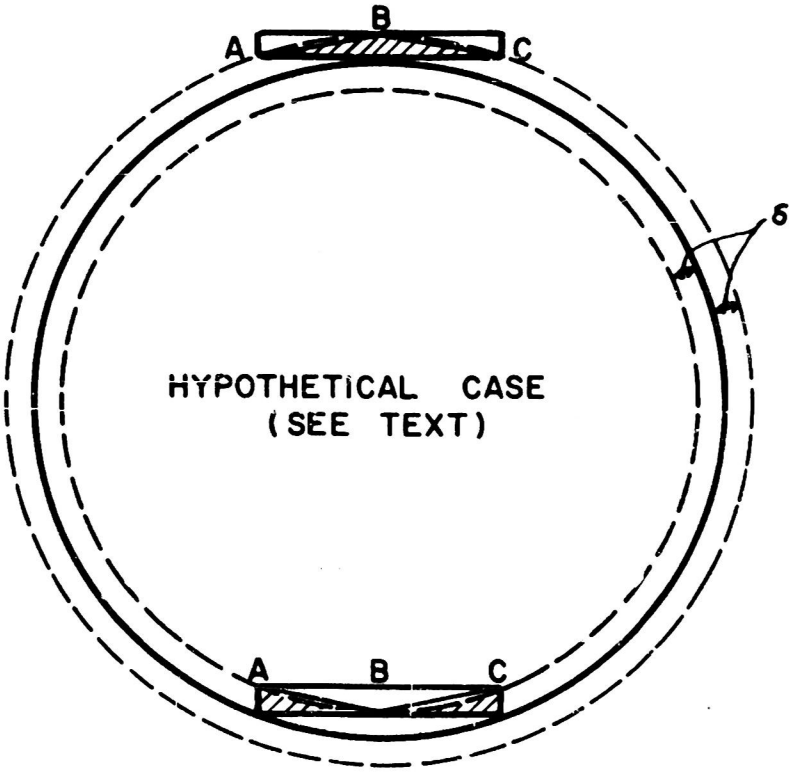

FIG. 5 PRESSURE PROBES (CONTINUED)

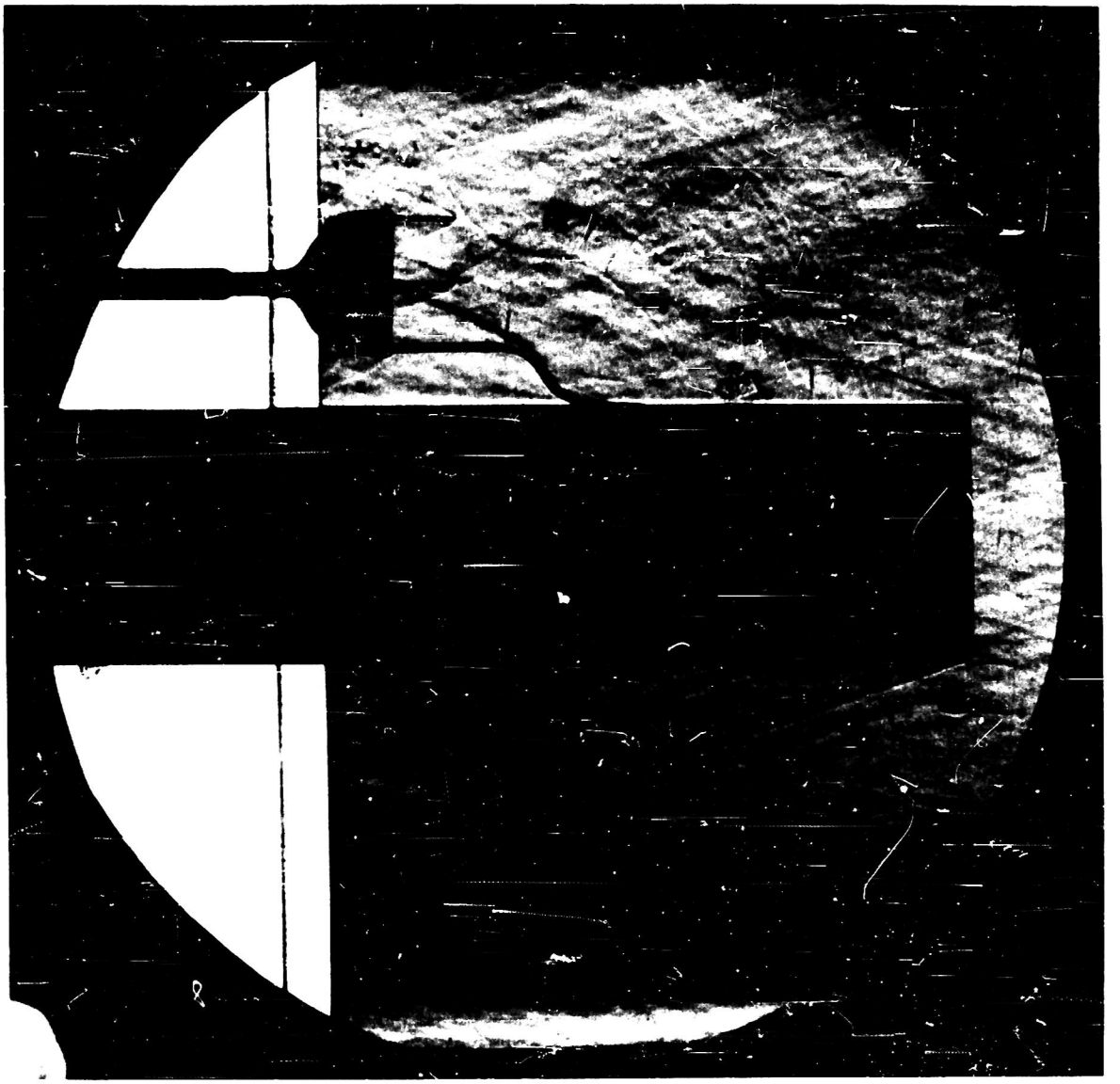

FIG. 6 SCHLIEREN PHOTOGRAPH OF FLOW ON MODEL WITH SURFACE PROBE AT M = 3.25

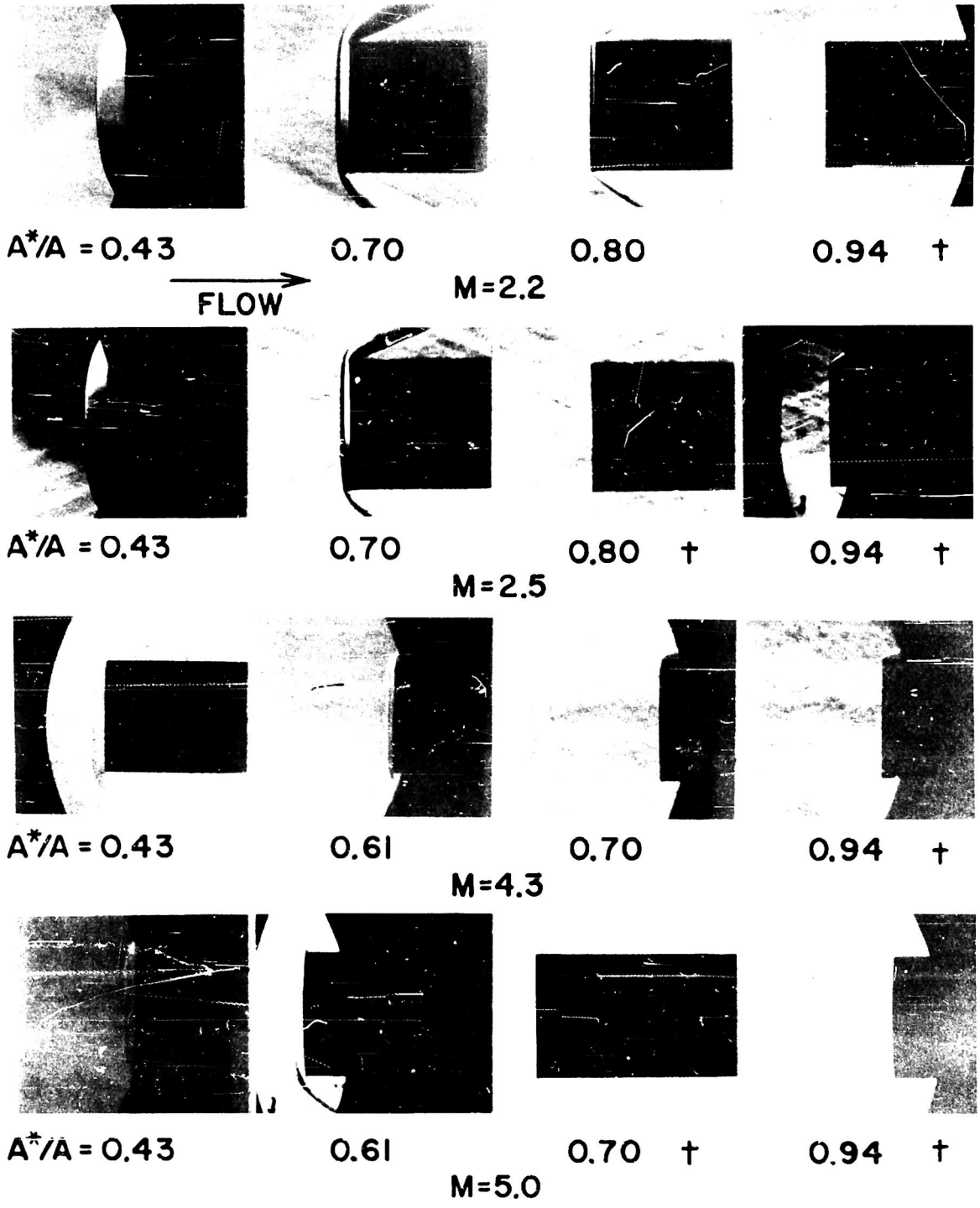

FIG. 7 PHOTOGRAPHS SHOWING EFFECT OF AREA RATIO ON THE "SWALLOWING" OF THE BOW SHOCK WAVE (+ SHOCK "SWALLOWED")

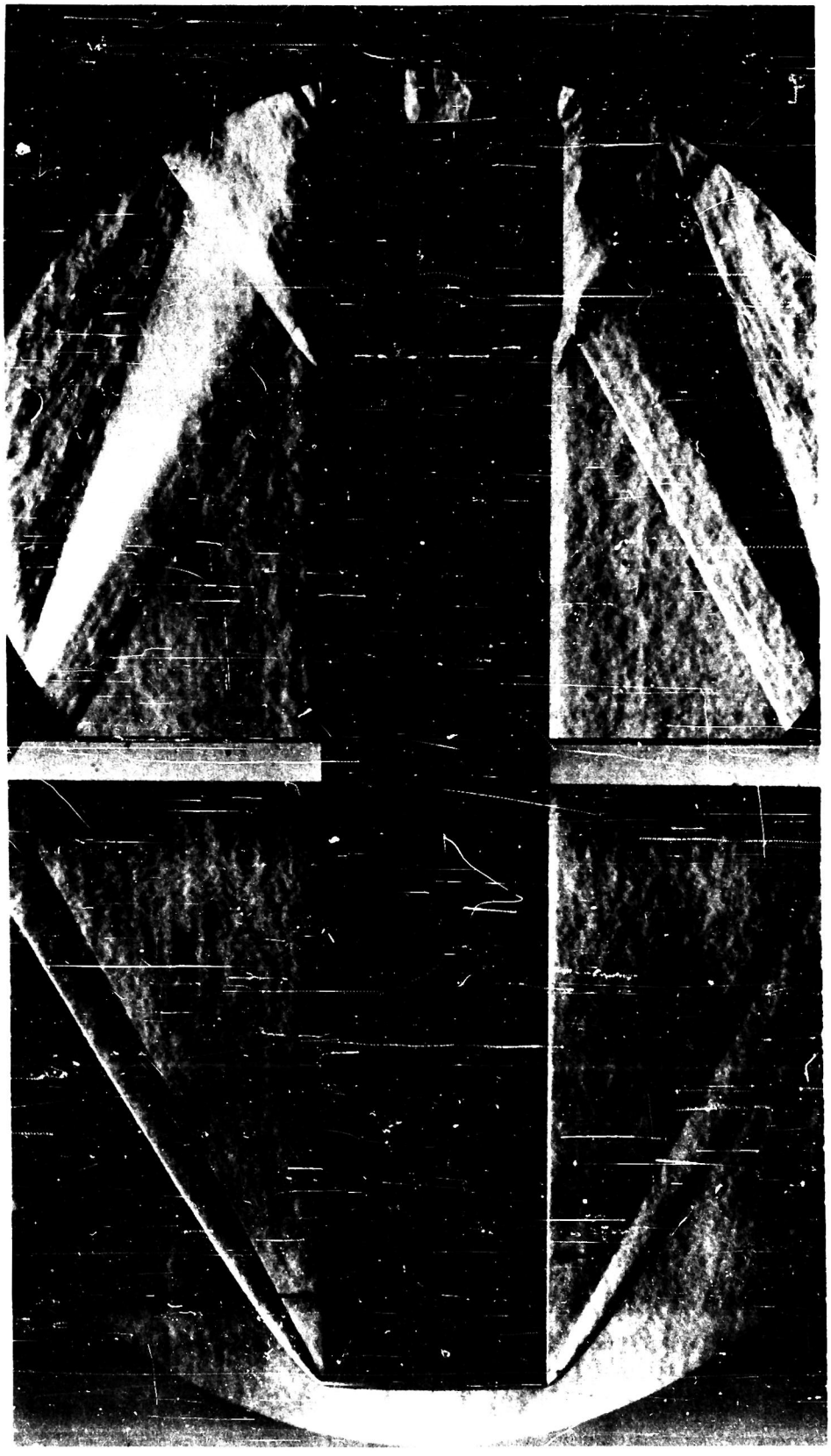

FIG. 8 SCHLIEREN PHOTOGRAPH OF INTERNAL BEVEL HOLLOW CYLINDER WITH BOW SHOCK NOT "SWALLOWED", M = 2.15

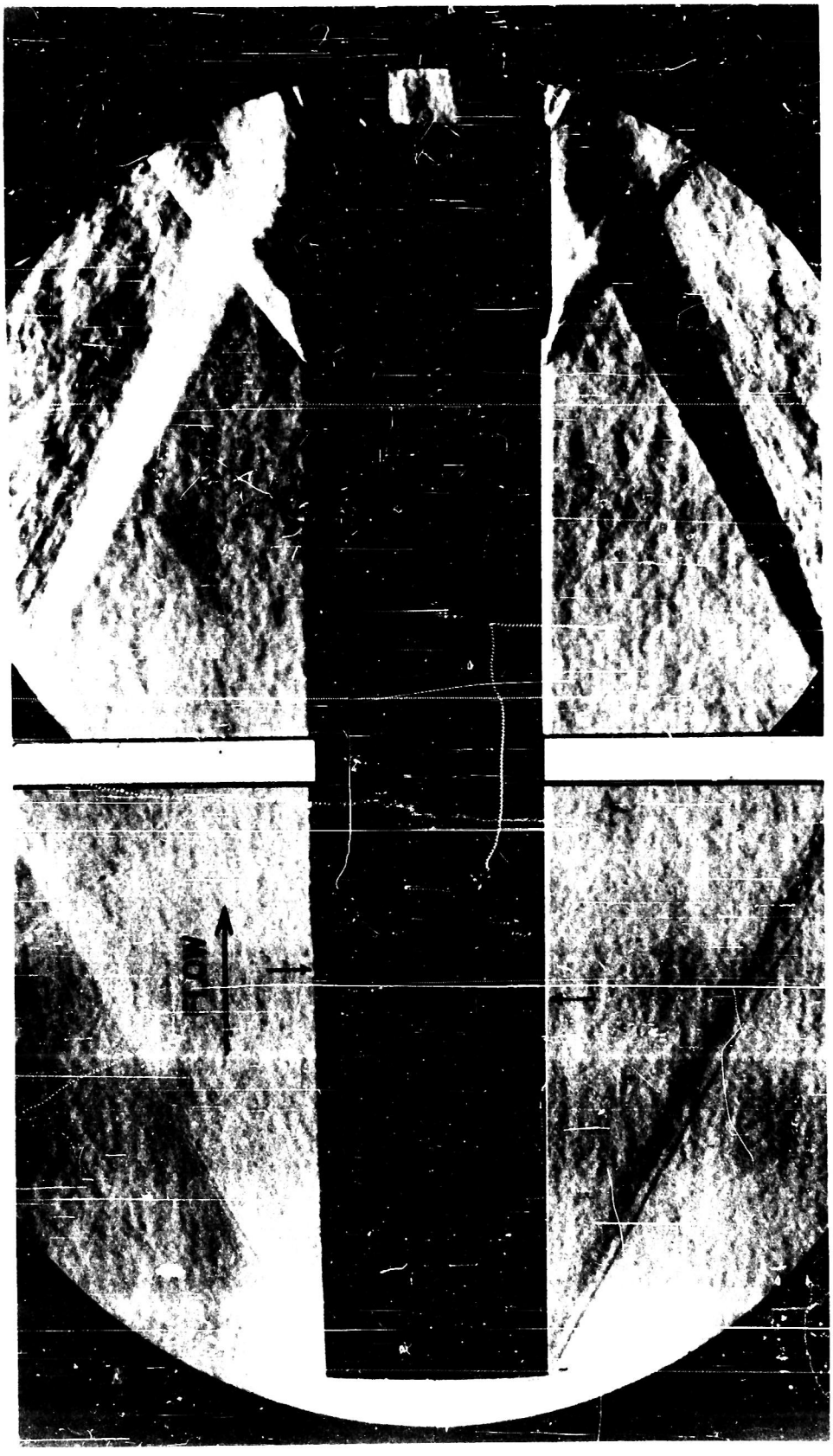

FIG. 9 SCHLIEREN PHOTOGRAPH OF INTERNAL BEVEL HOLLOW CYLINDER WITH BOW SHOCK "SWALLOWED", M = 2.15

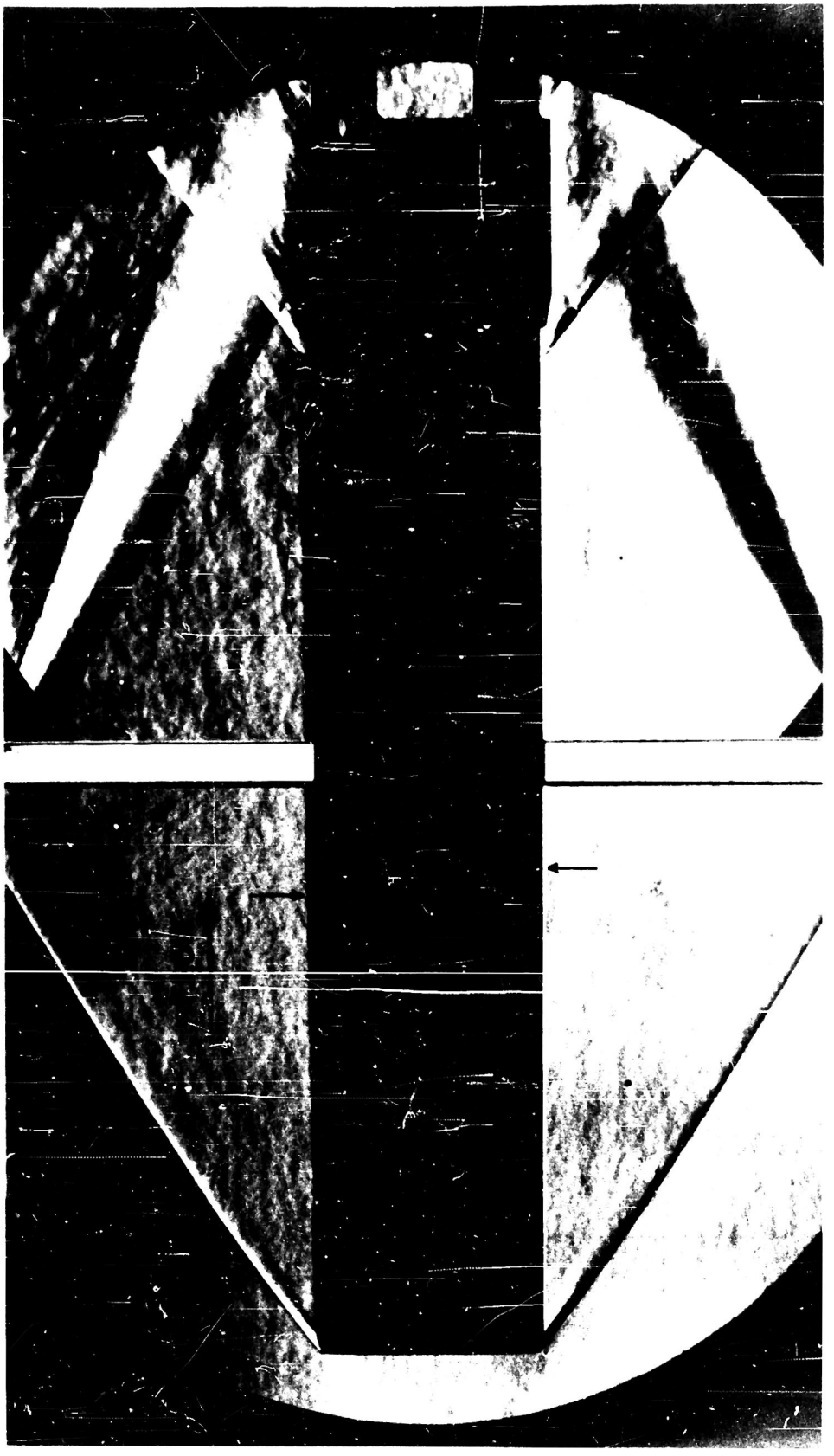

FIG. 10 SCHLIEREN PHOTOGRAPH OF EXTERNAL BEVEL HOLLOW CYLINDER WITH BOW SHOCK "SWALLOWED", M = 2.15

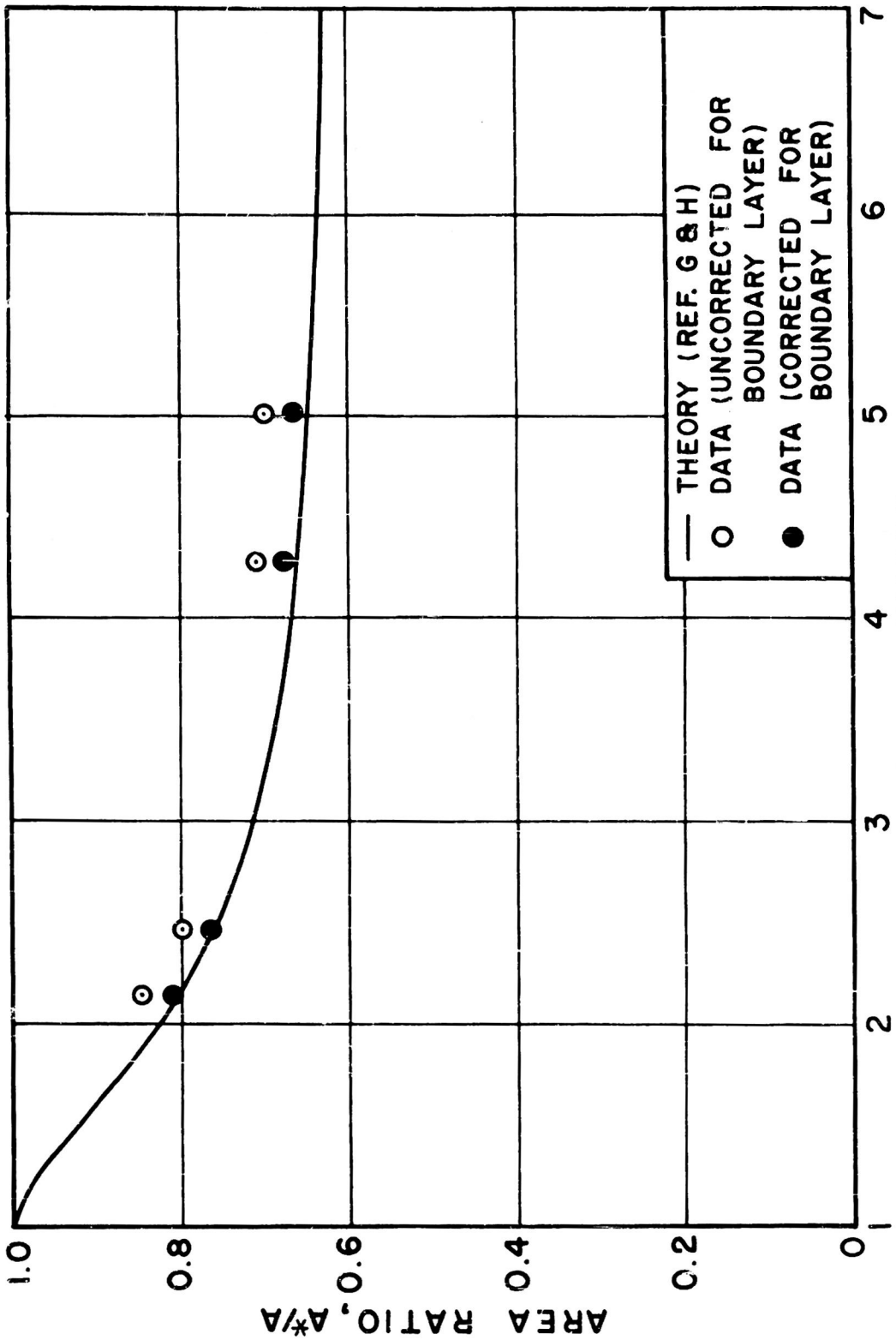

FIG. 11 MAXIMUM CONTRACTION RATIO TO "SWALLOW" BOW SHOCK

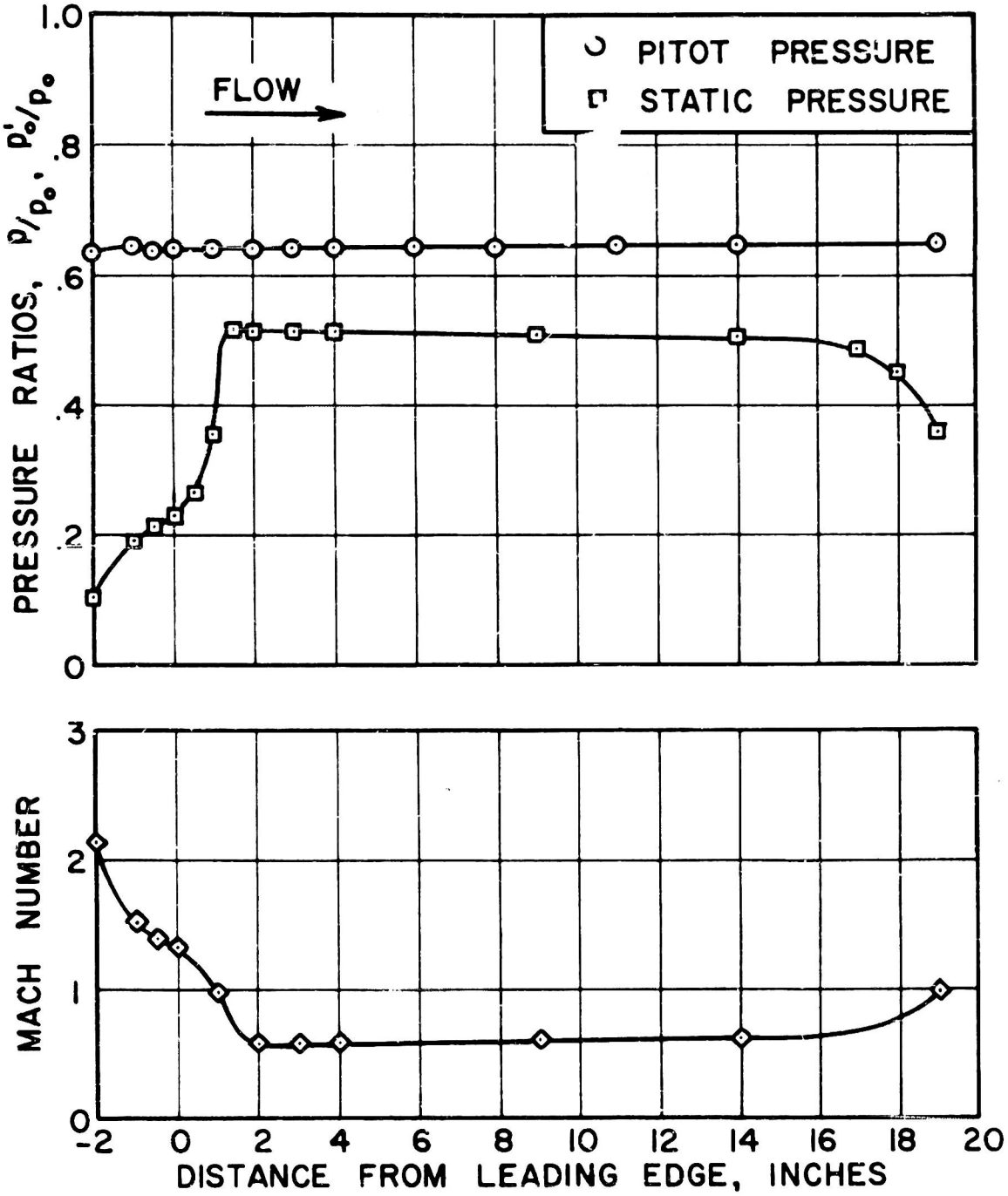

FIG. 12 PRESSURE AND MACH NUMBER DISTRIBUTION ALONG CENTERLINE OF HOLLOW CYLINDER WITH 10° INTERNAL BEVEL AND BOW SHOCK NOT "SWALLOWED", M=2.15

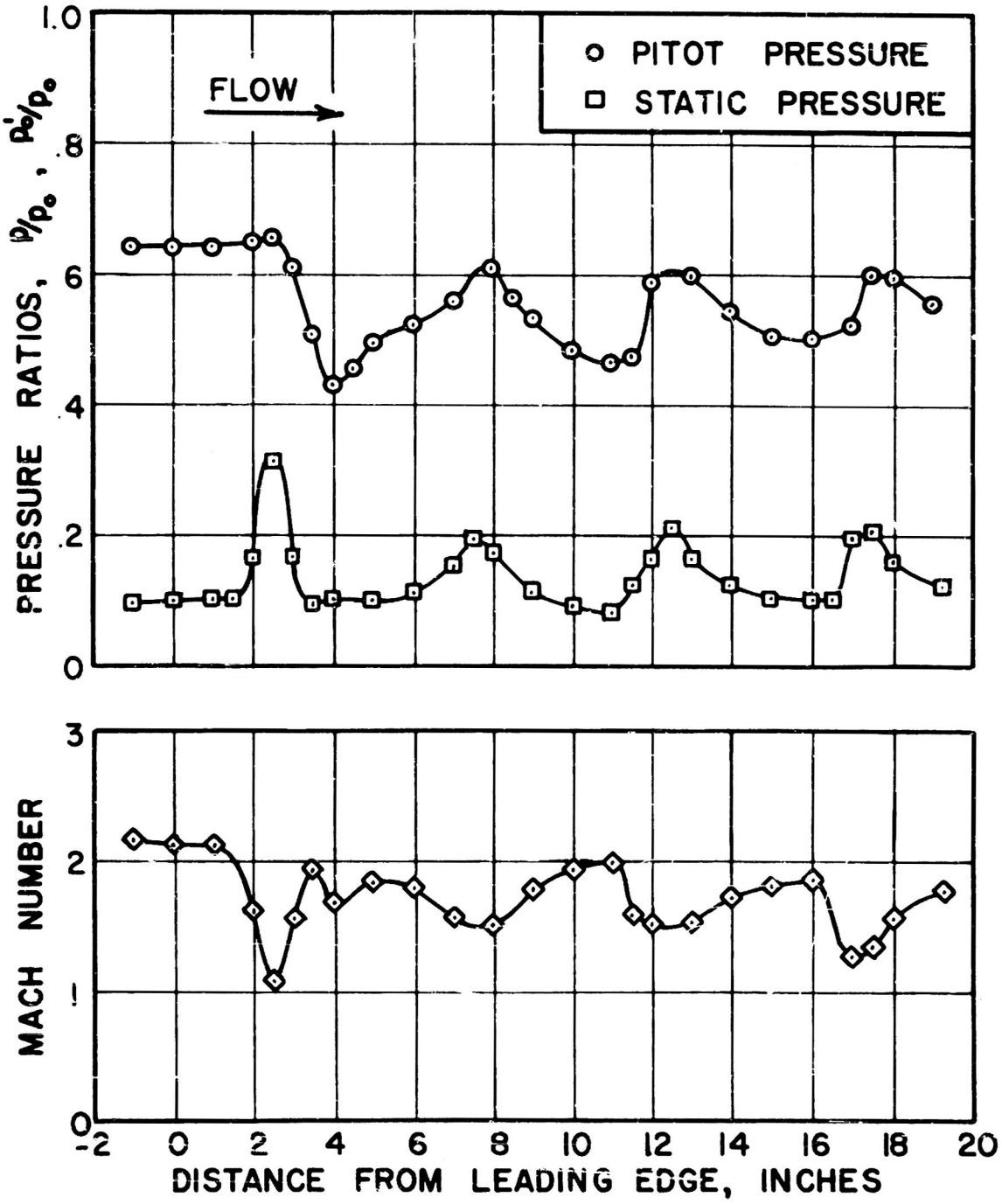

FIG. 13 PRESSURE AND MACH NUMBER DISTRIBUTION ALONG CENTERLINE OF HOLLOW CYLINDER WITH 10° INTERNAL BEVEL AND BOW SHOCK "SWALLOWED", M = 2.15

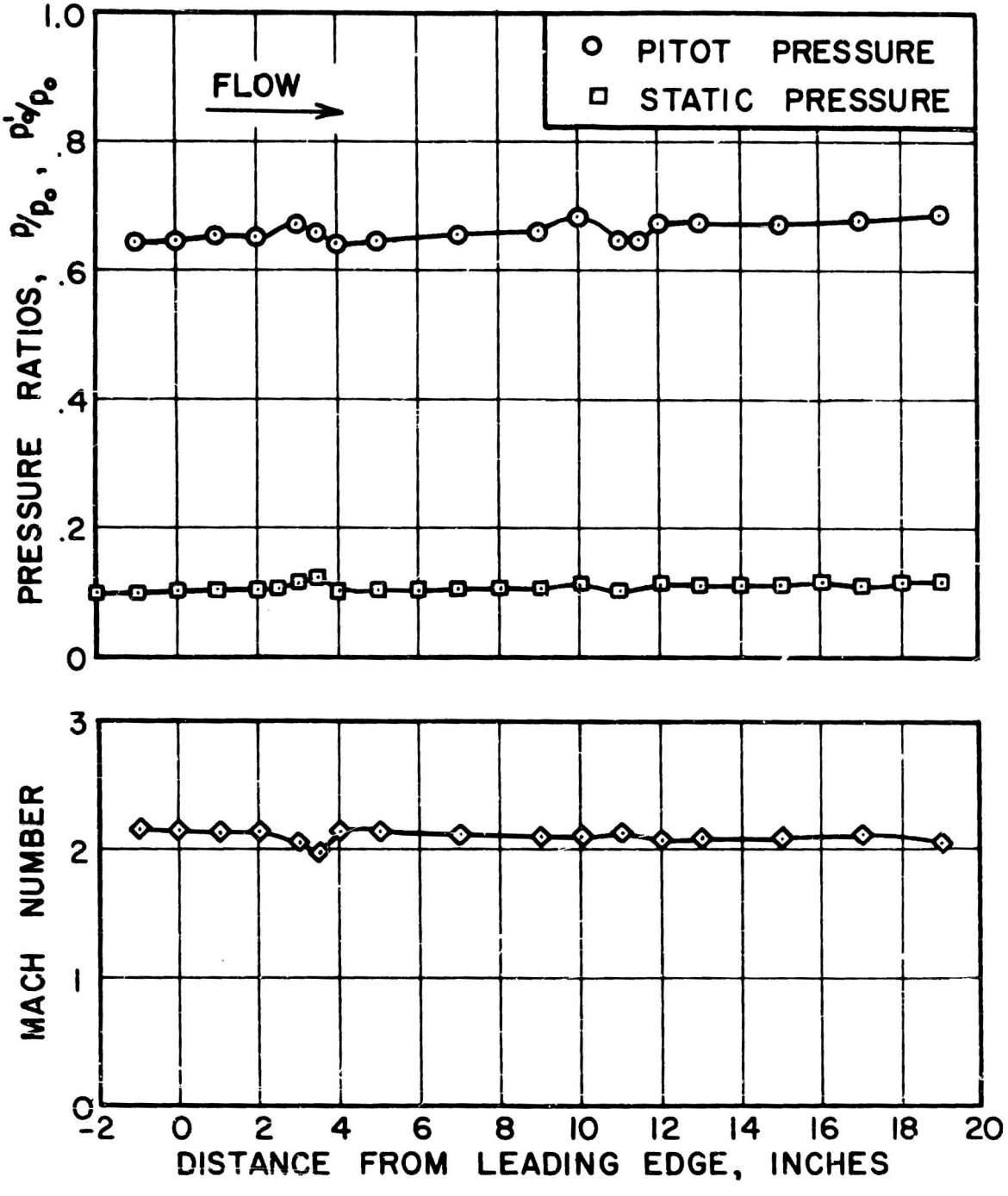

FIG. 14 PRESSURE AND MACH NUMBER DISTRIBUTION ALONG CENTERLINE OF HOLLOW CYLINDER WITH 10° EXTERNAL BEVEL AND BOW SHOCK "SWALLOWED", M = 2.15

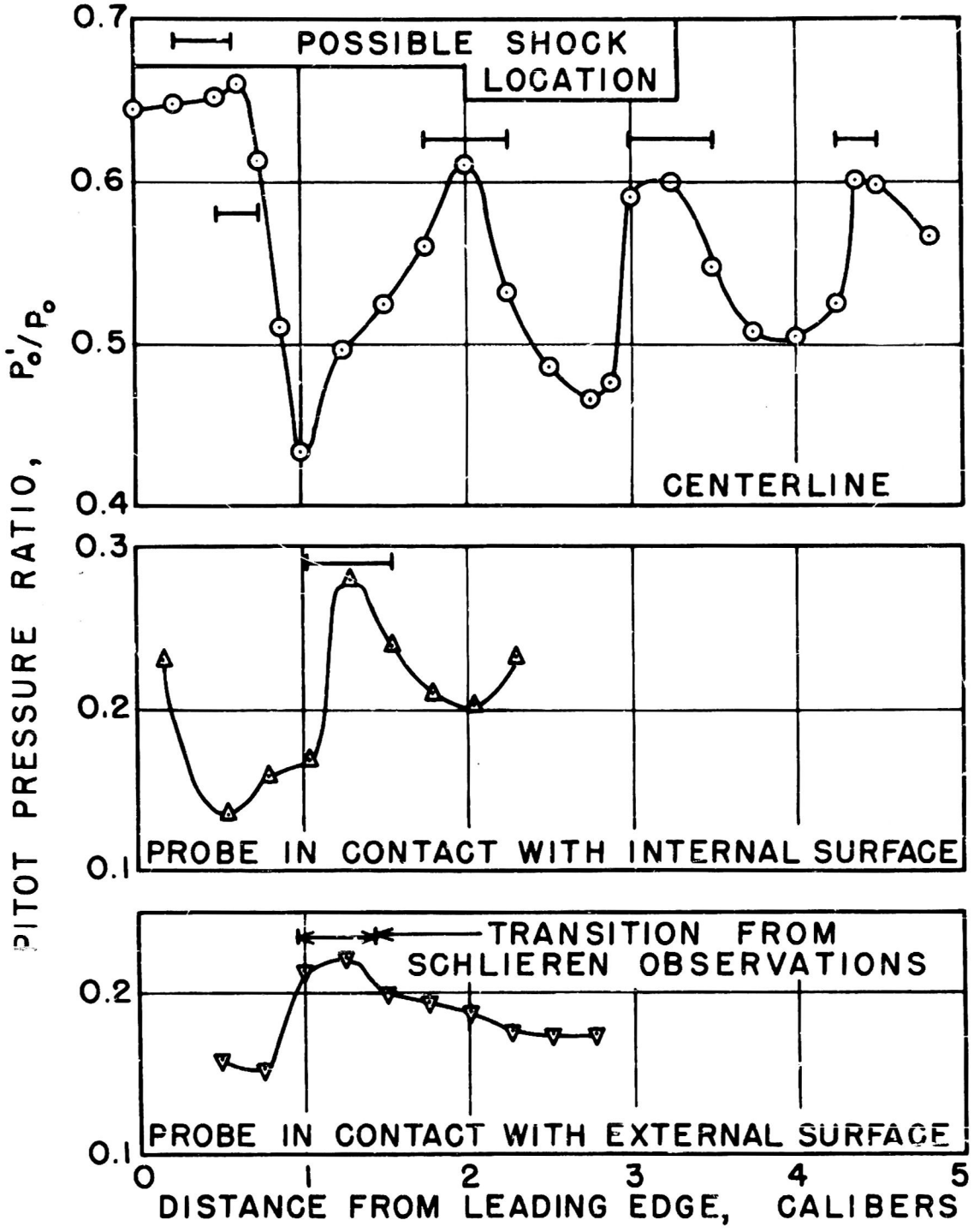

FIG. 15 PITOT PRESSURES ON INTERNAL BEVEL HOLLOW CYLINDER AT M = 2.15

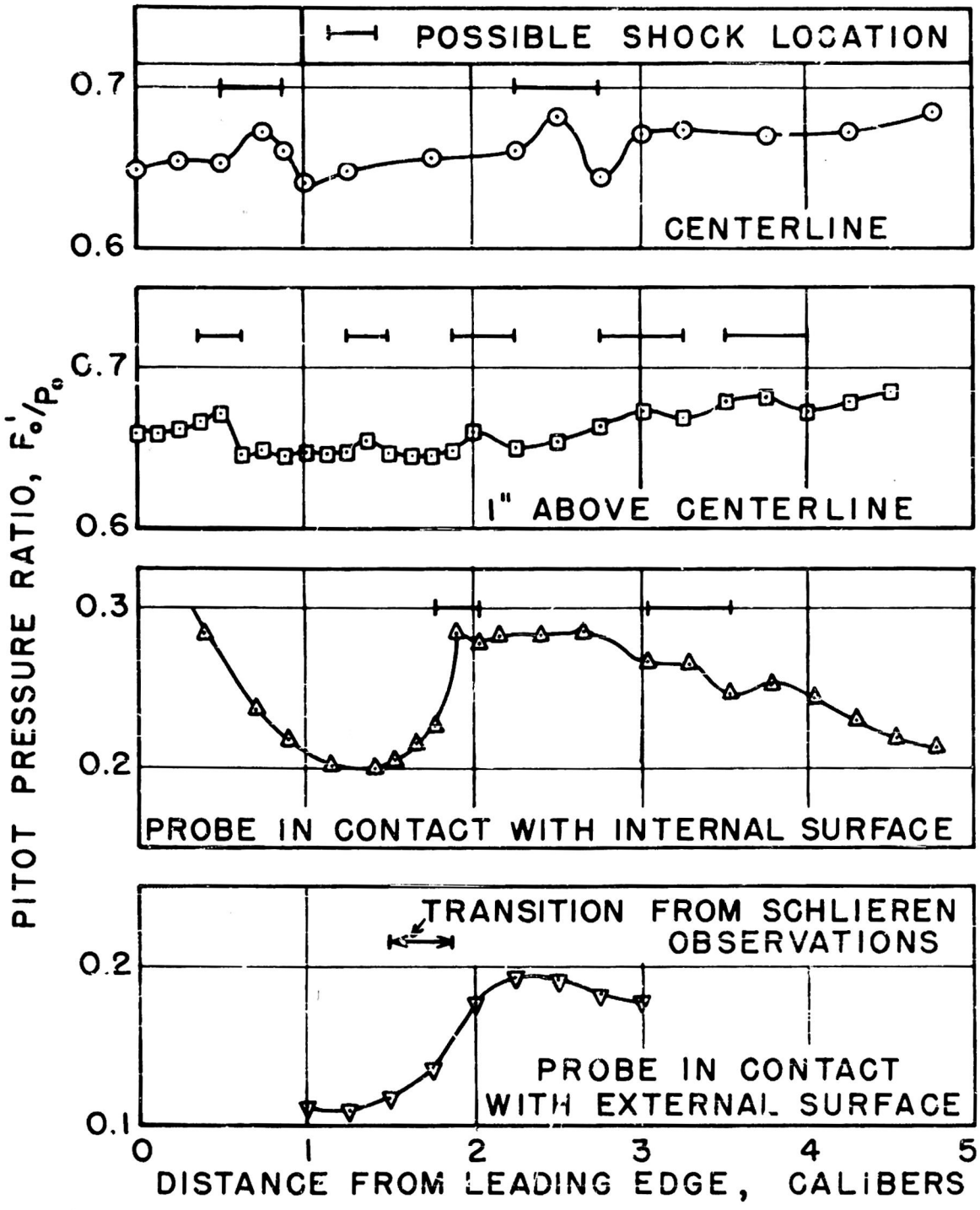

FIG. 16 PITOT PRESSURE ON EXTERNAL BEVEL HOLLOW CYLINDER AT M = 2.15

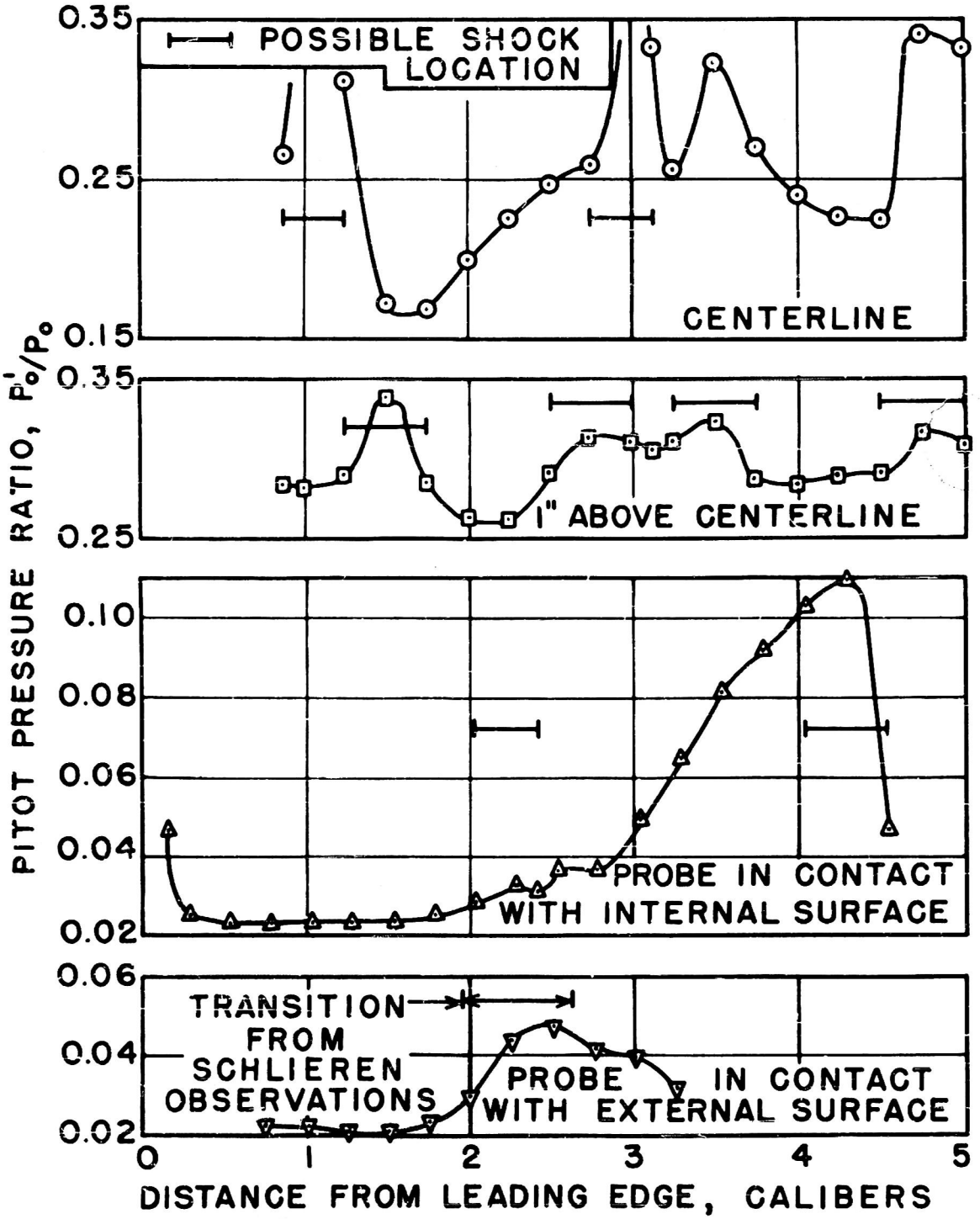

FIG. 17 PITOT PRESSURE ON INTERNAL BEVEL HOLLOW CYLINDER AT M = 3.25

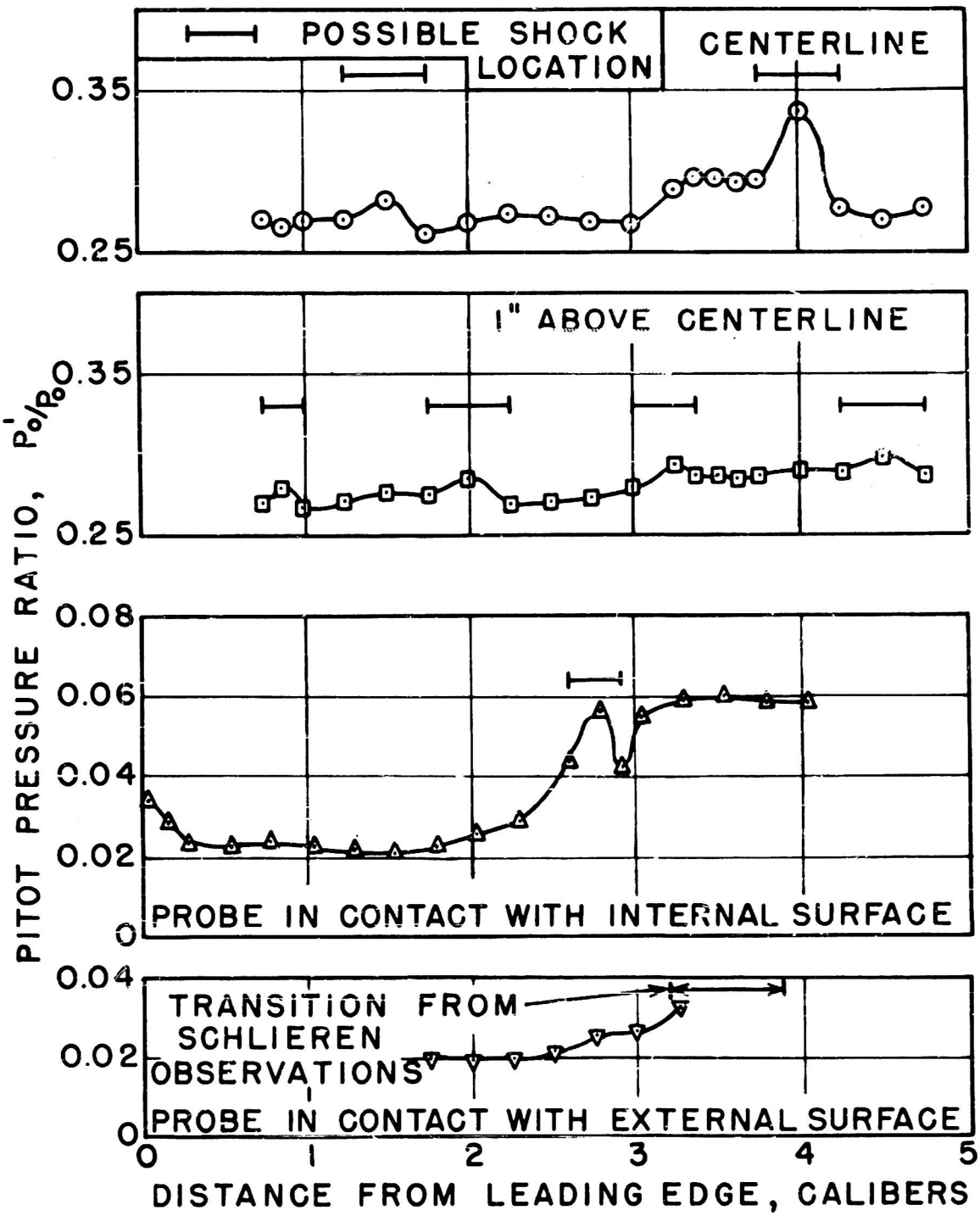

FIG. 18 PITOT PRESSURE ON EXTERNAL BEVEL HOLLOW CYLINDER AT M = 3.25

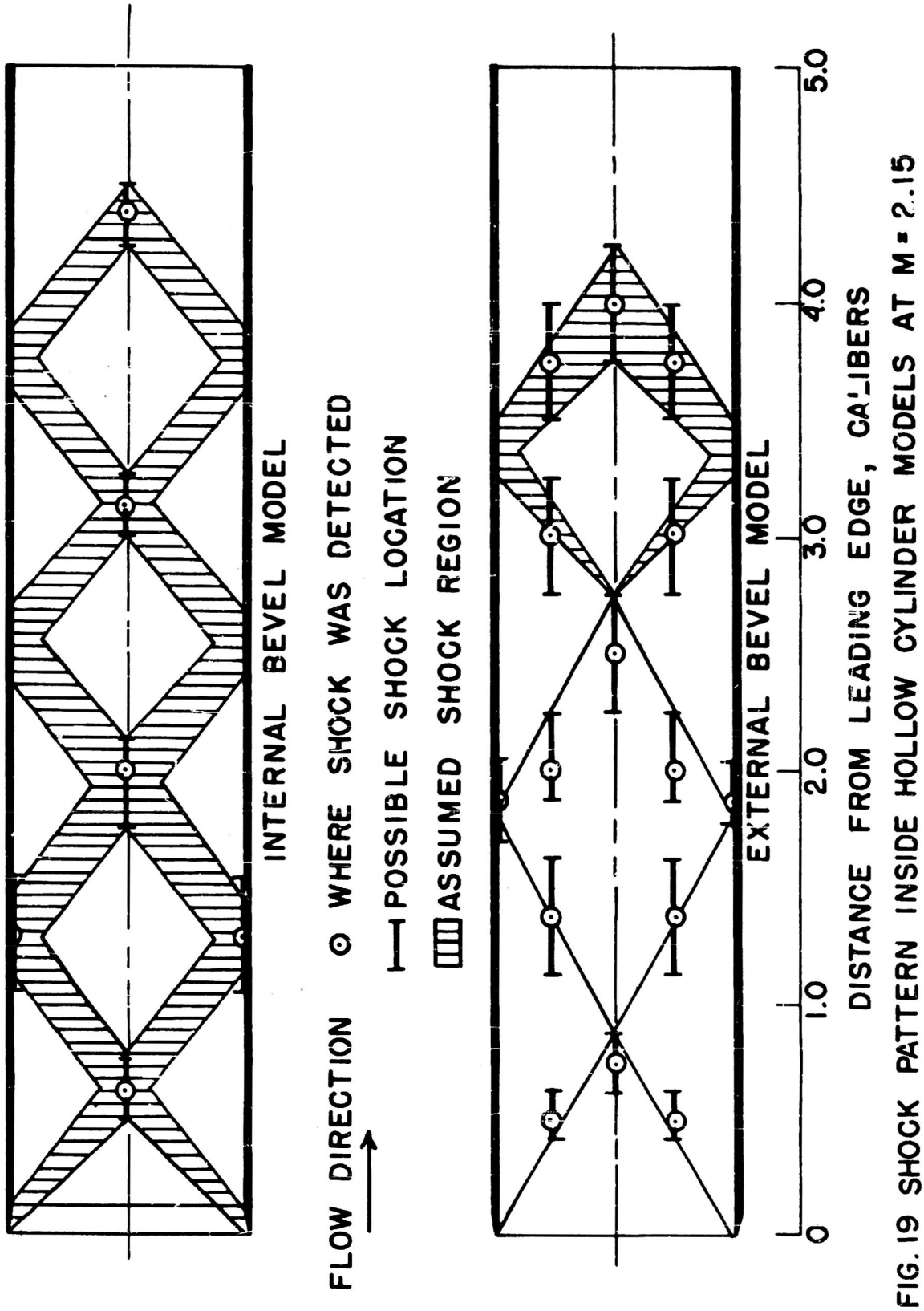

FIG. 19 SHOCK PATTERN INSIDE HOLLOW CYLINDER MODELS AT M = 2.15

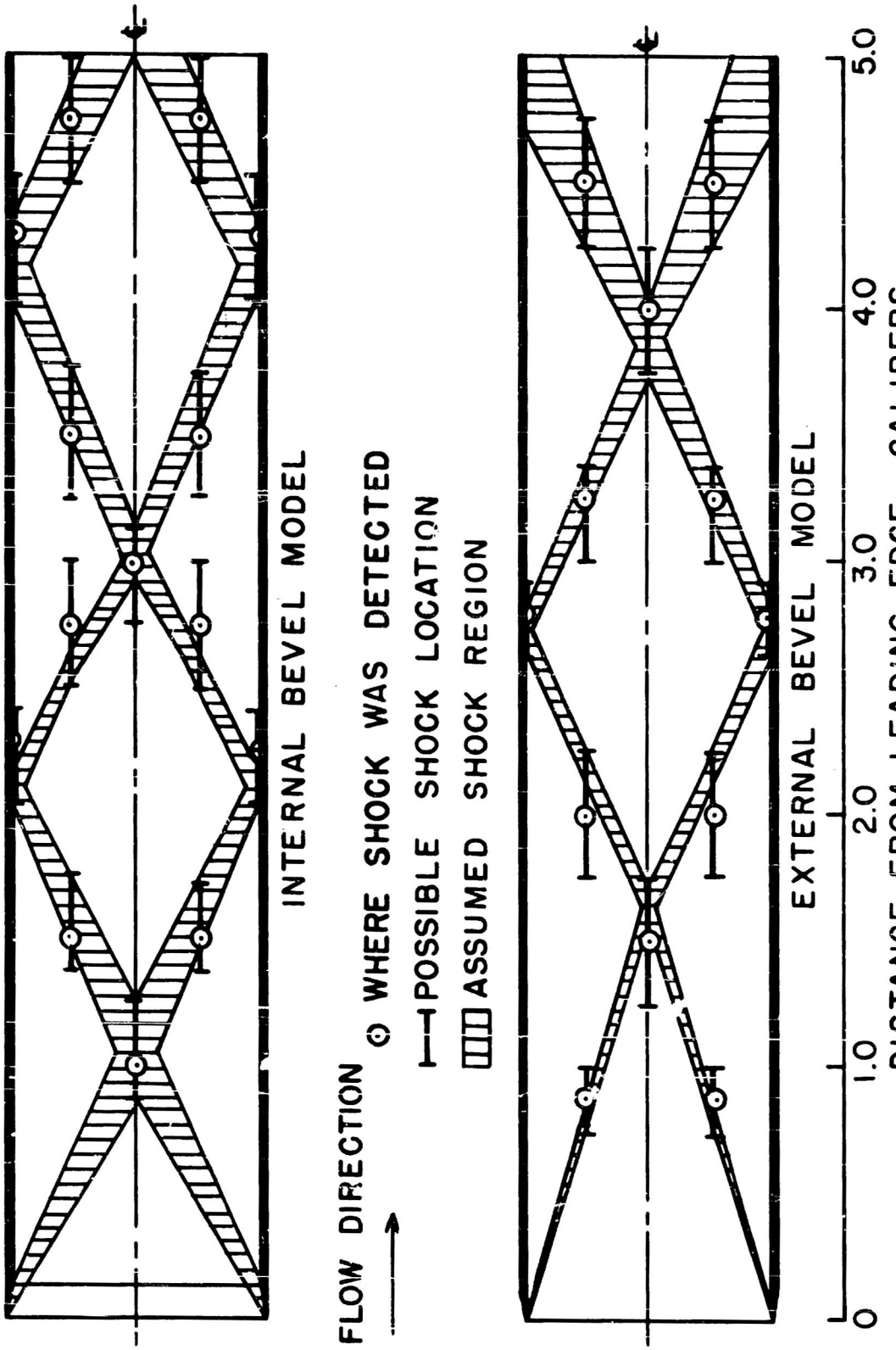

FIG.20 SHOCK PATTERN INSIDE HOLLOW CYLINDER MODELS AT M=2.25

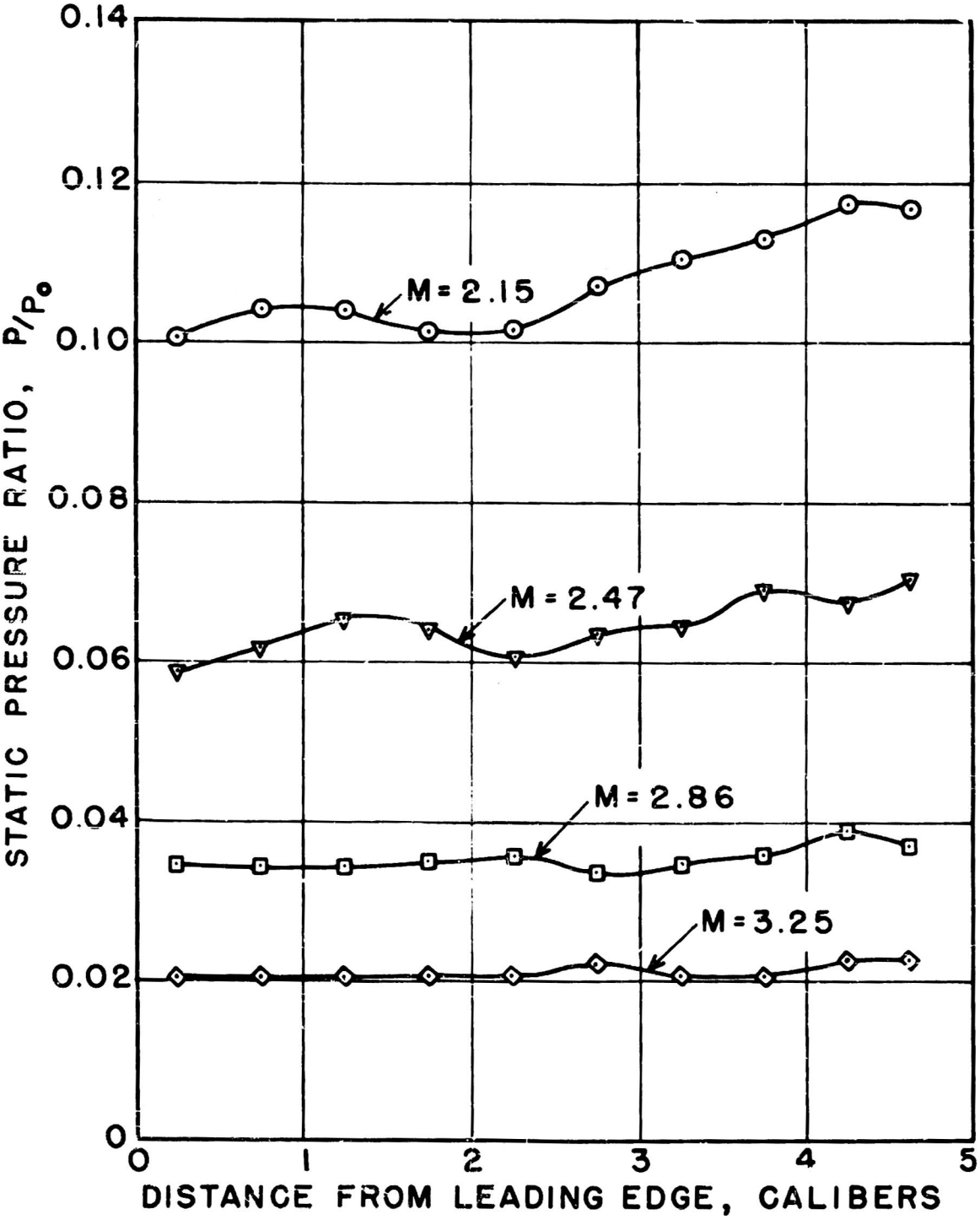

FIG. 21 STATIC PRESSURE DISTRIBUTION ON INTERNAL SURFACE OF EXTERNAL BEVEL MODEL

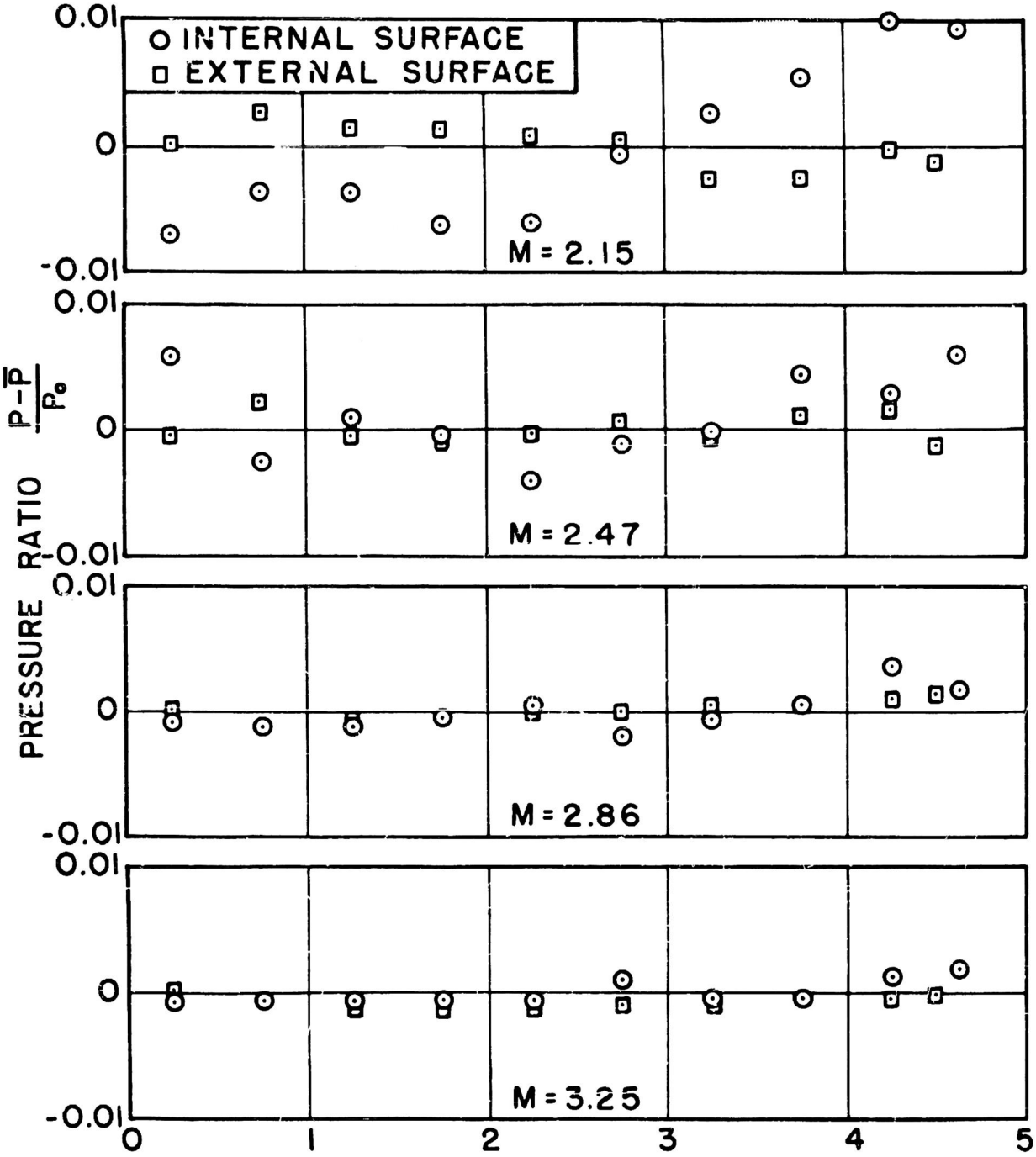

FIG. 22 COMPARISON OF STATIC PRESSURE ON INTERNAL SURFACE OF EXTERNAL BEVEL MODEL WITH EXTERNAL SURFACE OF INTERNAL BEVEL MODEL IN TERMS OF PRESSURE RATIO $\frac{P-\bar{P}}{P_o}$

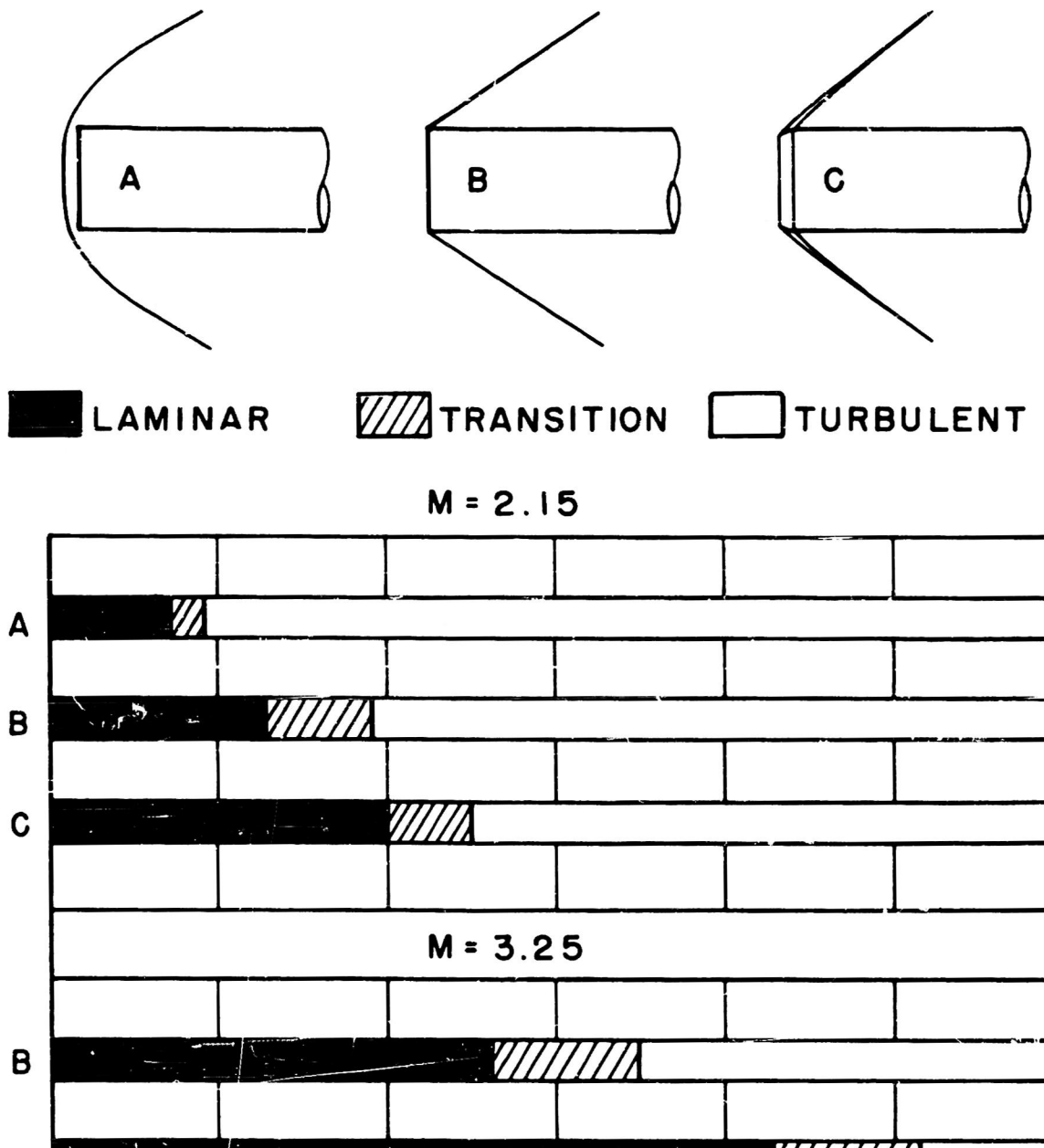

FIG. 23 COMPARISON OF BOUNDARY LAYER TRANSITION ON THE EXTERNAL SURFACE OF TWO DIFFERENT HOLLOW CYLINDER MODELS AT TWO MACH NUMBERS

Aeroballistic Research Department
External Distribution List for Aeroballistics Research (XI)

No. of Copies	
	Chief, Bureau of Ordnance Department of the Navy Washington 25, D.C.
1	Attn: Rea
1	Attn: Rexe
1	Attn: Re3d
2	Attn: Re6
3	Attn: Re9a
	Chief, Bureau of Aeronautics Department of the Navy Washington 25, D. C.
1	Attn: AER-TD-414
2	Attn: RS-7
	Commander U. S. Naval Ordnance Test Station Inyokern P.O. China Lake, California
2	Attn: Technical Library
1	Attn: Code 5003
	Commander U.S. Naval Air Missile Test Center Point Mugu, California
2	Attn: Technical Library
	Superintendent U.S. Naval Postgraduate School Monterey, California
1	Attn: Librarian
	Commanding Officer and Director David Taylor Model Basin Washington 7, D. C.
2	Attn: Hydrodynamics Laboratory
	Chief of Naval Research Library of Congress Washington 25, D. C.
2	Attn: Technical Info. Div.
	Office of Naval Research Department of the Navy Washington 25, D. C.
1	Attn: Code 438
2	Attn: Code 463
	Director Naval Research Laboratory Washington 25, D. C.
1	Attn: Code 2021
1	Attn: Code 3800
1	Officer-in-Charge Naval Aircraft Torpedo Unit U.S. Naval Air Station Quonset Point, Rhode Island
	Office, Chief of Ordnance Washington 25, D. C.
1	Attn: ORDTU

No. of Copies	
2	Library Branch Research and Development Board Pentagon 3D1041 Washington 25, D.C
	Chief, AFSWP P.O. Box 2610 Washington 25, D. C.
1	Attn: Technical Library
1	Chief, Physical Vulnerability Branch Air Targets Division Directorate of Intelligence Headquarters, USAF Washington 25, D. C.
	Commanding General Wright Air Development Center Wright-Patterson Air Force Base Dayton, Ohio
5	Attn: WCAPD
1	Attn: WCSD
2	Attn: WCSOR
2	Attn: WCRRN
1	Attn: WCACD
1	Attn: WCRRF
1	Director Air University Library Maxwell Air Force Base, Alabama
	Commanding General Aberdeen Proving Ground Aberdeen, Maryland
1	Attn: C.L. Poor
1	Attn: D.S. Dederick
	National Bureau of Standards Washington 25, D.C.
1	Attn: Nat'l Applied Math. Lab.
1	Attn: Librarian (Ord. Dev. Div.)
1	Attn: Chief, Mechanics Div.
	National Bureau of Standards Corona Laboratories (Ord. Dev. Div.) Corona, California
1	Attn: Dr. H. Thomas
	National Bureau of Standards Building 3U, UCLA Campus 405 Hilgard Avenue Los Angeles 24, California
1	Attn: Librarian
	University of California 211 Mechanics Building Berkeley 4, California
1	Attn: Dr. R. G. Folsom
1	Attn: Mr. G. J. Maslach
1	Attn: Dr. S. A. Schaaf VIA: InsMat

No. of Copies

California Institute of Technology
Pasadena 4, California
2 Attn: Librarian(Guggenheim Aero Lab)
1 Attn: Dr. H.T. Nagamatsu
1 Attn: Prof. M.S. Plesset
1 Attn: Prof. F. Goddard
1 Attn: Dr. Hans W. Liepman
VIA: BuAero Representative

College of Engineering
Cornell University
Ithaca, New York
1 Attn: Prof. A. Kantrowitz
VIA: ONR

University of Illinois
202 E. E. R. L.
Urbana, Illinois
1 Attn: Prof A. H. Taub
VIA: InsMat

1 Director
Inst. for Fluid Dynamics and Applied Math
University of Maryland
College Park, Maryland
VIA: InsMat

Massachusetts Inst. of Technology
Cambridge 39, Massachusetts
1 Attn: Prof. G. Stever
1 Attn: Prof. J. Kaye
VIA: InsMat

University of Michigan
Ann Arbor, Michigan
1 Attn: Prof. Otto Laporte
VIA: InsMat

University of Michigan
Willow Run Research Center
Ypsilanti, Michigan
1 Attn: L.R. Biasell
VIA: InsMat

University of Minnesota
Rosemount, Minnesota
1 Attn: J. Leonard Frame
1 Attn: Prof. N. Hall
VIA: Ass't InsMat

The Ohio State University
Columbus, Ohio
2 Attn: G. L. Von Eschen
VIA: Ass't InsMat

Polytechnic Institute of Brooklyn
99 Livingston Street
Brooklyn 2, New York
1 Attn: Dr. Antonio Ferri
VIA: ONR

Princeton University
Princeton, New Jersey
1 Attn: Prof. S. Bogdonoff
1 Attn: Prof. L. Lees
VIA: ONR

No. of Copies

Massachusetts Inst. of Technology
Cambridge 39, Massachusetts
2 Attn: Project Meteor
1 Attn: Guided Missiles Library

1 Princeton University
Forrestal Research Center Library
Project Squid
Princeton, New Jersey

Armour Research Foundation
35 West 33rd Street
Chicago 16, Illinois
1 Attn: Engr. Mech. Div.
VIA: ONR

Applied Physics Laboratory
The Johns Hopkins University
8621 Georgia Avenue
Silver Spring, Maryland
1 Attn: Arthur G. Norris
VIA: NIO

1 Cornell Aeronautical Lab., Inc.
4455 Genesee Street
Buffalo 21, New York
VIA: BuAero Rep.

1 Defense Research Laboratory
University of Texas
Box 1, University Station
Austin, Texas
VIA: InsMat

Eastman Kodak Company
50 W. Main Street
Rochester 4, New York
1 Attn: Dr. Herbert Trotter, Jr.
VIA: NIO

General Electric Company
Building #1, Campbell Avenue Plant
Schenectady, New York
1 Attn: Joseph C. Hoffman
VIA: InsMachinery

The Rand Corporation
1500 Fourth Street
Santa Monica, California
1 Attn: The Librarian
VIA: InsMat

Consolidated Vultee Aircraft Corp.
Daingerfield, Texas
1 Attn: J.E. Arnold
VIA: Dev. Contract Office

Douglas Aircraft Company, Inc.
3000 Ocean Park Boulevard
Santa Monica, California
1 Attn: Mr. E.F. Burton
VIA: BuAero Resident Rep.

No. of Copies

North American Aviation, Inc.
12214 Lakewood Boulevard
Downey, California
2 Attn: Aerophysics Library
VIA: BuAero Representative

United Aircraft Corporation
East Hartford 8, Connecticut
1 Attn: Robert C. Sale
VIA: BuAero Representative

National Advisory Committee for Aero
1724 F Street, Northwest
Washington 25, D. C.
5 Attn: E. B. Jackson

Ames Aeronautical Laboratory
Moffett Field, California
1 Attn: H.J. Allen
2 Attn: Dr. A.C. Charters

NACA Lewis Flight Propulsion Lab.
Cleveland Hopkins Airport
Cleveland 11, Ohio
1 Attn: John C. Evvard

Langley Aeronautical Laboratory
Langley Field, Virginia
1 Attn: Theoretical Aerodynamics Div.
1 Attn: J. V. Becker
1 Attn: Dr. Adolf Buseman
1 Attn: Mr. C. H. McLellan
1 Attn: Mr. J. Stack

Harvard University
21 Vanserg Building
Cambridge 38, Massachusetts
1 Attn: Prof. Garrett Birkhoff

The Johns Hopkins University
Charles and 34th Streets
Baltimore 18, Maryland
1 Attn: Dr. Francis H. Clauser

New York University
45 Fourth Avenue
New York 3, New York
1 Attn: Professor R. Courant

1 Dr. Allen E. Puckett, Head
Missile Aerodynamics Department
Hughes Aircraft Company
Culver City, California

1 Dr. Gordon N. Patterson, Director
Institute of Aerophysics
University of Toronto
Toronto 5, Ontario, Canada
VIA: BuOrd (Ad8)

Aeroballistic Research Department
External Distribution List for Aeroballistics Research (XIa)

No. of Copies	
6	Office of Naval Research Branch Office Navy 100 Fleet Post Office New York, New York
	Commanding General Aberdeen Proving Ground Aberdeen, Maryland
1	Attn: Dr. B.L. Hicks
	National Bureau of Standards Aerodynamics Section Washington 25, D.C.
1	Attn: Dr. G.B. Schubauer, Chief
	Ames Aeronautical Laboratory Moffett Field, California
1	Attn: Walter G. Vincenti
	University of California Observatory 21 Berkeley 4, California
1	Attn: Leland E. Cunningham VIA: InsMat
	Massachusetts Inst. of Technology Dept. of Mathematics, Room 2-270 77 Massachusetts Avenue Cambridge, Massachusetts
1	Attn: Prof. Eric Reissner VIA: InsMat
	Graduate School Aeronautical Engr. Cornell University Ithaca, New York
1	Attn: W.R. Sears, Director VIA: ONR
	Applied Math. and Statistics Lab. Stanford University Stanford, California
1	Attn: R.J. Langle, Associate Dir. VIA: Ass't InsMat
	University of Minnesota Dept. of Aeronautical Engr. Minneapolis, Minnesota
1	Attn: Professor R. Hermann VIA: Ass't InsMat
	Case Institute of Technology Dept. of Mechanical Engineering Cleveland, Ohio
1	Attn: Professor G. Kuerti VIA: ONR
	Harvard University 109 Pierce Hall Cambridge 38, Massachusetts
1	Attn: Professor R. von Mises

No. of Copies	
	Redstone Arsenal Huntsville, Alabama
1	Attn: Mr. J. L. Potter
1	Attn: Dr. L. W. Walter
	NACA Lewis Flight Propulsion Lab. Cleveland Hopkins Airport Cleveland, Ohio
1	Attn: Dr. H. S. Ribner
1	Attn: Mr. P. F. Brinich